AD-A104 558 IOWA UNIV IOWA CITY DEPT OF PHYSICS AND ASTRONOMY F/G 4/1
PLASMA WAVES NEAR THE MAGNETOPAUSE.(U)
JUN 81 R R ANDERSON, C C HARVEY, M M HOPPE N00014-76-C-0016
UNCLASSIFIED U. OF IOWA-81-25 NL

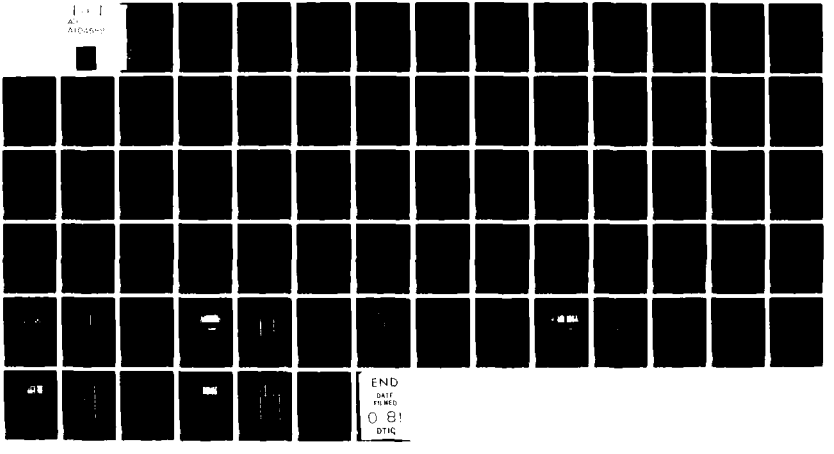

END
DATE FILMED
08!
DTIC

U. of Iowa 81-25

(10)

Department of Physics and Astronomy

THE UNIVERSITY OF IOWA

Iowa City, Iowa 52242

U. of I. 81-25

Plasma Waves Near the Magnetopause

by

R. R. Anderson[1], C. C. Harvey[2], M. M. Hoppe[3],
B. T. Tsurutani[4], T. E. Eastman[1] and J. Etcheto[5]

June, 1981

Department of Physics and Astronomy
The University of Iowa
Iowa City, IA 52242

Submitted for publication to Journal of Geophysical Research

1. Department of Physics and Astronomy, University of Iowa, Iowa City, Iowa 52242
2. Observatoire de Paris, Section d'Astrophysique, 92190 Meudon, France
3. Institute of Geophysics and Planetary Physics, University of California, Los Angeles, California 90024
4. Jet Propulsion Laboratory, 4800 Oak Grove Drive, Pasadena, California 91109
5. CRPE/CNET, 92131 Issy-les-Moulineaux, France

SECURITY CLASSIFICATION OF THIS PAGE (When Data Entered)

REPORT DOCUMENTATION PAGE		READ INSTRUCTIONS BEFORE COMPLETING FORM
1. REPORT NUMBER U. of Iowa 81-25	2. GOVT ACCESSION NO. AD-A104	3. RECIPIENT'S CATALOG NUMBER 558
4. TITLE (and Subtitle) Plasma Waves Near the Magnetopause		5. TYPE OF REPORT & PERIOD COVERED Research June 1981
		6. PERFORMING ORG. REPORT NUMBER
7. AUTHOR(s) R. R. Anderson, C. C. Harvey, M. M. Hoppe, B. T. Tsurutani, T. E. Eastman and J. Etcheto		8. CONTRACT OR GRANT NUMBER(s) N00014-76-C-0016, NAS5-2
9. PERFORMING ORGANIZATION NAME AND ADDRESS Department of Physics and Astronomy The University of Iowa Iowa City, Iowa 52242		10. PROGRAM ELEMENT, PROJECT, TASK AREA & WORK UNIT NUMBERS
11. CONTROLLING OFFICE NAME AND ADDRESS Office of Naval Research Electronics Program Office Arlington, Virginia 22217		12. REPORT DATE June 1981 13. NUMBER OF PAGES 70
14. MONITORING AGENCY NAME & ADDRESS(if different from Controlling Office)		15. SECURITY CLASS. (of this report) UNCLASSIFIED 15a. DECLASSIFICATION/DOWNGRADING SCHEDULE

16. DISTRIBUTION STATEMENT (of this Report)

Approved for public release; distribution is unlimited.

17. DISTRIBUTION STATEMENT (of the abstract entered in Block 20, if different from Report)

18. SUPPLEMENTARY NOTES

To be published in Journal of Geophysical Research

19. KEY WORDS (Continue on reverse side if necessary and identify by block number)

Magnetopause
Plasma Waves

20. ABSTRACT (Continue on reverse side if necessary and identify by block number)

(See page following)

DD FORM 1 JAN 73 1473 EDITION OF 1 NOV 65 IS OBSOLETE
S/N 0102-LF-014-6601

UNCLASSIFIED
SECURITY CLASSIFICATION OF THIS PAGE (When Data Entered)

ABSTRACT

Plasma waves associated with the magnetopause, from the magnetosheath to the outer magnetosphere, are examined with an emphasis on high-time resolution data and the comparison between measurements using different antenna systems. An early ISEE crossing of the magnetopause region including passage through two well-defined flux transfer events, the magnetopause current layer and boundary layer plasma is studied in detail. The waves in these regions are compared and contrasted to the waves in the adjoining magnetosheath and outer magnetosphere. Four types of plasma wave emissions are characteristic of the nominal magnetosheath: 1) a very low frequency continuum; 2) short wavelength spikes; 3) "festoon-shaped" emissions below about 2kHz; and 4) "lion roars". The latter two emissions are well correlated with ultra-low frequency magnetic field fluctuations. The dominant plasma wave features during flux transfer events are 1) an intense low frequency continuum which includes a substantial electromagnetic component; 2) a dramatic increase in the frequency of occurrence of the spikes; 3) quasi-periodic electron cyclotron harmonics correlated with ~ 1 Hz magnetic field fluctuations; and 4) enhanced electron plasma oscillations. The plasma wave characteristics in the current layer and in the boundary layer are quite similar to the features in the flux transfer events. Upon entry into the outer magnetosphere, the plasma wave spectra are dominated by intense electromagnetic chorus bursts and electrostatic $(n + 1/2)f_g^-$ emissions. Wavelength determinations made by comparing the various antenna responses and polarization measurements for the different waves are also presented.

I. INTRODUCTION

In this paper we attempt to characterize the waves seen in association with the magnetopause, from the magnetosheath to the outer magnetosphere. For this we have studied in detail an early ISEE crossing of the magnetopause region, including passages through two well defined flux transfer events (FTE's), the magnetopause current layer and boundary layer plasma. We compare and contrast the waves seen in these regions and in the adjoining magnetosheath and outer magnetosphere.

The period studied is the magnetopause crossing on the inbound leg on ISEE orbit no. 7 on November 8, 1977. This period was selected because: 1) it includes examples of most of the magnetopause associated phenomena observed on other ISEE passes; 2) the ISEE spacecraft were in high bit rate mode during this pass, giving the best possible time resolution: 3) the data quality is good; 4) ISEE 1 and 2 were close together; and 5) being early in the mission, the individual ISEE experimenters have already analyzed and reported on their data for this time period in some detail: Elphic and Russell (1979), Frank et al. (1978), Ogilvie and Scudder (1979) Paschmann (1979), Paschmann et al. (1978), and Russell and Elphic (1978). The principal current sheet was crossed by ISEE 1 between 02:50 and 02:51 U.T., when the spacecraft was at a geocentric distance of 11.2 R_E, at a geomagnetic latitude of 0° and at 11.4 hours magnetic local time. The observed sheath magnetic field was directed at an angle about 50° below the equatorial plane (Russell and

Elphic, 1978) just preceding the magnetopause crossing, but earlier it was closer to the equatorial plane.

The objectives of this study are fourfold: 1) to obtain a clearer definition or description of the boundaries and regions we are studying; 2) to characterize the waves observed in these regions; 3) to determine which wave modes are present; and, if possible, 4) to determine their origin. Much has already been learned about plasma waves near the magnetopause in the initial studies of Gurnett et al. (1979b) and Tsurutani et al. (1981a). This report expands on these original studies by concentrating on high-time resolution observations and by comparing and contrasting the data obtained using the different antenna systems on ISEE 1 and 2. After a brief description of the instrumentation, we follow the spacecraft through the successive regions encountered as they pass from the magnetosheath to the magnetosphere.

II. INSTRUMENTATION

The principal ISEE instruments used in this study are the University of Iowa Plasma Wave Experiment (Gurnett et al., 1978, 1979a) on ISEE 1 (GUM) and ISEE 2 (GUD), the Observatoire de Paris - CRPE Electron Density Experiment (Harvey et al., 1978, 1979) (HAM) and the UCLA Fluxgate Magnetometer Experiment (Russell, 1978) on ISEE 1 (RUM). High-time resolution measurements on the ISEE 1 plasma wave (GUM) experiment are obtained from the electric and magnetic spectrum analyzers and the wideband receiver. For this study the electric spectrum analyzer and the wideband receiver are connected to the 215 m tip-to-tip Heppner long wire antenna. The electric spectrum analyzer has 20 narrowband channels logarithmically spaced from 5.6 Hz to 311 kHz and the magnetic spectrum analyzer - which is connected to the spin-axis search coil magnetometer - has 14 channels from 5.6 Hz to 10 kHz. The channels below 10 kHz have bandwidths about ± 15% of their center frequencies and the channels at 10 kHz and above have bandwidths about ± 7.5% of their center frequencies. The dynamic range of the spectrum analyzers is about 110dB and the time constant of the compressors is about 50 ms. In the high bit rate mode all the spectrum analyzer channels are sampled simultaneously every 0.25 s. The ISEE 2 Plasma Wave (GUD) Experiment has a single 16-channel spectrum analyzer covering the frequency range from 5.6 Hz to 31.1 kHz with the same filter characteristics as the ISEE 1 spectrum analyzers. For this study, the ISEE 2 spectrum analyzer is connected to the 30 m

tip-to-tip electric dipole antenna. The wideband receivers on both spacecraft are operating in the d.c.-10kHz mode.

The French electron density experiment measures the electron density by two complementary techniques (Harvey et al., 1978): a resonance sounder aboard ISEE 1 (HAM) and a wave propagation experiment between ISEE 1 and 2 (HAD). The activity of both experiments is controlled by their duty cycle, which is decided by the ISEE Science Working Team; in this study, we are concerned only with data obtained from the sounder when it is passive. During the period we consider here, the sounder receiver is connected to the Mozer antenna. Designed primarily for d.c. field measurements, the sensor consists of a pair of spheres, at the ends of a pair of cables of overall (sphere-to-sphere) length 73.5 m deployed in the spacecraft spin plane perpendicular to the Heppner antenna. Preamplifiers situated in the spheres drive the input differential amplifier of the HAM experiment. The sounder receiver has a bandwidth of 400 Hz, and at this time, the frequency synthesizer is stepping the center of the receiver band through the frequency range 0.47 to 50.65 kHz in 128 frequency steps. The receiver output is sampled every 15.625 ms. The synthesizer rests for 125 ms on each frequency step, giving seven points (the eighth is used for engineering data) per frequency step, and 16 s for a complete frequency sweep. The comparison of data from the two radio receivers (GUM and HAM) is important for two reasons: the different frequency and time resolutions, and the different types of antennas used.

ISEE 1 and 2 carry identical triaxial fluxgate magnetometers with flippers which enable sensor offsets to be determined accurately. Data used in this study are taken in the high sensitivity mode, where the

range is ± 256nT. The three components of the field are sampled 512 times per second and averaged digitally in overlapped "box-car" averages to provide a 16-bit measurement with an exact zero in its transfer function at the Nyquist frequency. This feature minimizes the effects of signals outside the analysis frequency band on signals inside that band. Data used in this study are taken at high bit rate when the magnetometer output rate is 16 vectors per second, corresponding to a Nyquist frequency of 8 Hz.

III. DATA ANALYSIS

The magnetic field data in this study are plotted in boundary normal coordinates. The boundary normal coordinate system has been previously discussed by Russell and Elphic (1978). The current layer structure observed at this inbound magnetopause crossing is consistent with the identification of the boundary as a tangential discontinuity. The coordinate system used in this work relies on this identification and is based on a boundary normal, defined as the cross-product of the observed fields on either side of the boundary (Siscoe et al., 1967), as is appropriate for such a discontinuity: this is the N-direction and it points outwards along the magnetopause normal. The L-direction is along the projection of the solar magnetospheric Z direction perpendicular to the normal. The M-direction completes the right-handed orthogonal set and points roughly opposite to the direction of the earth's rotation. The L, M, N vectors thus obtained for this magnetopause are, in GSE corrdinates, L = (-.312, -.235, .921), M = (-.116, -.952, -.282), and N = (.943, -.195, .270).

All electric field strengths quoted here are calculated by dividing the measured potential difference at the antenna preamplifier inputs by the antenna effective length, which is assumed to be half the tip-to-tip length for the dipole antenna and equal to the distance betwen the spheres for the double sphere antenna. While the field strengths obtained by the two experiments usually agree, there are occasions, which particularly concern the present study, where the calculated field strengths are obviously different. This we attribute

to the difference of antenna design and dimensions, and in parts of this study, to quantitatively compare the measurements on the two antennas, we have averaged both the GUM and HAM data to make the receivers look as similar to each other as is possible. This is especially important because, as will be seen, the emissions have much fine structure in the frequency-time domain.

Consider the ISEE 1 frequency-time plane between 0.5 and 50.6 kHz during any period of 16 s. The GUM multi-channel spectrum analyzer can be thought of as sampling the whole of the area of the frequency-time domain by making 64 measurements at each of eight logarithmically spaced frequency intervals between 0.56 and 31.1 kHz. (This is not strictly true, because the detector time constant is 50 ms, whereas the sampling period is much longer, 250 ms). The HAM receiver, on the other hand, samples the frequency-time plane only inside a narrow area 125 ms wide running diagonally across the given 50 kHz x 16 s domain; however, inside this narrow area, both frequency and time resolution are greater than for GUM. To make the HAM frequency response comparable with GUM, HAM channels near each GUM frequency are averaged after weighting by the GUM filter response function. Thus, the GUM 562 Hz channel is compared directly with the average of the seven samples in the HAM 469 HZ channel, while the GUM 31.1 kHz channel is compared with the weighted average of the samples in the 32 HAM channels nearest 31.1 kHz.

While HAM is averaged in frequency, GUM is sampled and averaged in time. Thus, the HAM 469 Hz channel is compared with the GUM 562 Hz sample occurring nearest in time to the HAM frequency step; and the HAM frequency-averaged 31.1 kHz is compared with the weighted time-average of the 16 GUM 31.1 kHz channel samples nearest in time to the 32 HAM

samples; the weighting function is similar to that used for the frequency average, but is applied to only half the number of samples, because there is only one GUM sample for every two HAM frequency steps.

IV. OBSERVATIONS

To give an overview of the data we are studying, Figure 1 shows a plot of the most important magnetic field and plasma parameters needed for understanding the relative location of the ISEE 1 spacecraft with respect to the magnetopause on the inbound orbit on November 8, 1977. During the whole of this passage, ISEE 2 was less than 370 km from ISEE 1, and corresponding plots for ISEE 2 can be found in Russell and Elphic (1978), Paschmann et al. (1978) and Frank et al. (1978).

A. The Nominal Magnetosheath

From 0202 to 0212 U.T., 0215 to 0230 U.T., and 0238 to 0240 U.T., the spacecraft was in the magnetosheath under conditions which appear to be fairly typical of the late morning sector. In these three time intervals, the sheath magnetic field was southward of the ecliptic plane by, respectively, about 5°, 0°, and from 20° to 50°.

Figure 2 shows 5 minutes of data collected in the magnetosheath from 0224 to 0229 U.T. The only selection criteria was that the data in this time period were typical of the entire magnetosheath on this pass. The top panels show the high time resolution GUM electric and magnetic spectrum analyzer data; the middle panel shows the magnetic field magnitude; and the bottom panels show the electric field outputs from the GUM and HAM receivers, averaged respectively in time and frequency as described in Section III. The data gap in the spectrum analyzer data is due to the HAM sounder having two active sweeps. On both sweeps, short time constant resonances were seen above about 38 kHz on about half the frequency steps when the antenna was at a large

inclination to the magnetic field. We interpret these as Bernstein mode wave resonances occurring at harmonics of the rapidly fluctuating electron gyrofrequency. Their intensity distribution suggests that the local plasma frequency is somewhat above the upper limit, 50.6 kHz, of the sounder frequency sweep, indicating a density somwhat above 31 cm^{-3}. This is consistent with the LASL/MPE fast plasma instrument ion density plotted in Figure 1.

The magnetometer data show the presence of fluctuations with a period of 20-40 seconds. Figure 1 shows that these magnetic fluctuations are evident on this orbit throughout the magnetosheath. Because most of the field variation is in field magnitude, a minimum variance direction (which can be a plane for purely compressive structures) may not correspond to a direction of propagation. A proper method of determining the direction of propagation can be found in Tsurutani et al. (1981b). In that article the fluctuations are shown to be compressible and the observed density fluctuations are anti-correlated with $|B|$. These properties indicate the fluctuations could be entropy fluctuations convecting past the spacecraft or slow-mode magneto-acoustic waves. Tsurutani et al. (1981b) argue that most probably these fluctuations are slow-mode magneto-acoustic waves propagating nearly perpendicular to the ambient magnetosheath magnetic field. For later reference, we note that the magnetic field does not have any higher frequency (especially ~1 Hz) components to its spectrum.

The spectrograms at the top of Figure 3 show data from the wideband receiver which aid us in identifying the various waves present in Figure 2. Four types of regular or steady emissions can be identified:

1) A low frequency continuum which is present nearly all the time;
2) Spikes which appear as thin vertical lines occurring randomly at

any time and which extend over the whole frequency range from about 100 Hz to above 10 kHz. In fact, the digital data in Figure 2 show that they extend up to as high as 56 kHz. Although the spikes are predominantly electrostatic, the data in Figure 2 show that brief electromagnetic bursts near the electron gyrofrequency occur coincident with the more intense spikes. The spikes are a permanent feature of the nominal magnetosheath on this passage and are the main contribution to the average spectrum above a few kHz. The HAM passive sounder data show that they are of very brief duration. At a fixed frequency, their e-folding time is often comparable to or shorter than the HAM sounder AGC time constant, which is 8 ms. The electric spectrum analyzer digital data show that to within the 50 ms resolution of the receiver, they occur simultaneously over the entire frequency range. Their origin is presently unknown;

3) "Festoon-shaped" electrostatic emissions over the frequency range below about 2 kHz. Unlike the first two types of emissions, these emissions are correlated with the low frequency magneto-acoustic waves; they occur only in the low p (high $|B|$) phase of the waves. These emissions consist of rising and falling tones with a frequency drift rate of about 1 kHz/s. The festoons tend to repeat at a period of about 1.5 s, one-half the spacecraft spin period. The higher frequency portion of the emission occurs when the electric dipole antenna is aligned most nearly perpendicular to the ambient magnetic field; and

4) "lion roars" first identified by Smith et al. (1969), which are also correlated with the low frequency magneto-acoustic waves. Smith and Tsurutani (1976) demonstrated that the nearly monochromatic electromagnetic emissions propagate along $\vec{B}$ and are correlated with decreases in the field magnitude. The electromagnetic "lion roars" occur during

the high β (low $|B|$) portion of the wave in the frequency range from about 50 Hz to 200 Hz. These whistler-mode waves have been studied in greater detail by Tsurutani et al. (1981b) who have shown that they are generated by an electron cyclotron instability driven by a temperature anisotropy. A fifth type of emission only occasionally observed appears to consist of narrowband emissions occurring at harmonics of the electron cyclotron frequency, as for example, at 0227:42, 0227:54 and at 0227:56 U.T. We have not found evidence of these emissions correlating with the magneto-acoustic waves, particle intensities or any plasma parameters.

By comparing the electric and magnetic spectrum analyzer data in Figure 2, one sees that the spikes, "festoon-shaped" emissions and the electron cyclotron harmonics are predominantly electrostatic, while the "lion roars" and the low frequency continuum are electromagnetic. Refractive index measurements made from the magnetic to electric field strength ratios show that the "lion roars" measurements are in good agreement with parallel propagating whistler mode waves, but that the low frequency continuum must have an additional electrostatic component. This component is probably a result of the solar array interference which affects the lower frequency electric channels.

The GUM-HAM comparison at the bottom of Figure 2 shows that for most of the time in most of the frequency channels, the HAM output indicates that any received signal is below the antenna noise level. Exceptions to this are the 5.6 kHz and 10 kHz channels, where the spikes cause some measurable signals and in the 562 Hz and 1 kHz channels, where the "festoon-shaped" emissions are noticeably above the noise level. At these times, the apparent signal strengths obtained from the double sphere antenna are higher than from the long wire

antenna; closer examination shows that this is indeed real and not an artifact of the higher noise level on this antenna.

Figure 4 shows the mean square average, minimum and maximum electric field strengths observed during the period 0224:00 to 0229:00 U.T.; this period is basically the same as is used in Figure 2, except that it is adjusted to obtain an integral number of frequency sweeps of the HAM experiment. Both the GUM and HAM noise levels used throughout this paper were determined during this five minute period of nominal magnetosheath. The GUM electric and magnetic field noise levels agree approximately with those published by Gurnett et al. (1978). For HAM it was found that, except for the very few frequency steps where emissions were observed, the minimum, average and maximum observed field strengths were stable and consistent with random noise measured with a receiver of 400 Hz bandwidth and 8 ms detector time constant; in particular, the minimum signal is some 3 dB below the mean noise level. At frequencies near 10 kHz, the mean noise level is significantly (4 dB) higher than it was in the solar wind earlier during the same orbit. It is clear that, for both experiments, the average field should be interpreted with some caution.

In his study of magnetosheath electrostatic turbulence, Rodriguez (1979) found that there were typically three components which could be identified in the spectra: a high frequency component peaking at the electron plasma frequency, a low-frequency component below the ion plasma frequency with a broad intensity maximum and an intermediate component between the ion and electron plasma frequencies. In Figure 4, we observe similar spectra with a few additional features. In this

time interval f_g^-, the electron cyclotron frequency, varied from 400 Hz to 1 kHz; f_p^-, the electron plasma frequency, varied from 50 to 56 kHz; and f_p^+, the ion plasma frequency, varied from 1.15 to 1.3 kHz. The feature between 56 Hz and 178 Hz is due to the electromagnetic "lion roars". Below 100 Hz, interference from the solar array dominates the spectrum. From about the ion plasma frequency up to the electron plasma frequency, the main contribution to the magnetosheath spectrum comes from the spikes. From the peak spectra, it is evident that the field strengths of the spikes are comparable and higher as measured on ISEE 2 and the Mozer antenna than as measured on the Heppner antenna. This indicates wavelengths less than 215 m.

A polarization analysis program developed primarily for use on data with higher electric field strengths has been applied to the HAM data with interesting results. The program averages the square of the electric field measured in some selected frequency range for each of 18 different 10° increments of the antenna phase in its spin plane, measured with respect to the projection of the magnetic field into the spin plane. When this analysis was performed on 15 minutes of HAM quiet magnetosheath data betwen 0216 and 0231 U.T., the mean electric field in the range 1.7 to 20.2 kHz was found to peak sharply when the antenna was at spin phase 140° ± 5°. During this period, the mean magnetic field ecliptic longitude was about 260° ± 5°, implying that the electric field peaks at ecliptic longitude 40 or 220°, which is close to the plasma flow direction of 208°. When all signals above 4×10^{-13} $V^2m^{-2}Hz^{-1}$ (31 points) were eliminated and the polarization analysis repeated, a quasi-sinusoidal spin modulation was found with the minimum when the antenna is perpendicular to the magnetic field.

Similar results, but without the peak at 220°, are obtained with the GUM experiment; the maximum field strength in the 5.6 kHz channel is observed when the Heppner antenna is most nearly parallel to the ambient magnetic field.

B. Flux Transfer Events

Flux transfer events are three dimensional field structures often encountered in the neighborhood of the magnetopause and which appear to be reconnected flux tubes which are being lifted out of the magnetosphere proper and are being pulled tailwards through their connection to the convecting magnetosheath field. They were first identified by Russell and Elphic (1978) on the basis of their magnetic field signatures, which include a characteristic variation in B_N, first to large positive values, then to negative values and finally back to zero. These authors also found that while the bulk plasma during flux transfer events resembled magnetosheath plasma with enhanced flow velocities, bursts of energetic electrons and protons apparently of magnetospheric origin were also associated with the flux transfer events. Further study of the bulk plasma and energetic particle characteristics during flux transfer events has been carried out by Paschmann et al. (1978), Frank et al. (1978) and Parks et al. (1979, 1981).

On the inbound magnetopause pass presently under discussion, two flux transfer events can be seen. The first flux transfer event is shown in Figure 5. As this flux transfer event is one of the prototype events studied by Elphic and Russell (1979), the magnetic field in boundary normal coordinates has already been discussed and is shown here as being the best way to characterize the spacecraft's progress

through the event. The event has the characteristic large positive B_N excursion followed by a large negative B_N excursion and then a return to near zero.

As shown in Figure 1, increased fluxes of energetic ions (5.1 keV -27 keV) were observed by the Frank experiment (FRM) on ISEE 1 to begin at ~0212 U.T., peak at ~0213 U.T. and return to their previous level by ~0216 U.T. The fluxes of energetic electrons (E > 45 keV) observed by FRM began a sharp rise at 0212:12 U.T., peaked at 0213:39 U.T. and returned to their previous levels by 0214:47 U.T. The timing differences between the electrons and ions are not significant because the ion measurements have much poorer time resolution. We have displayed the FRM ion data because, although it has poorer time resolution, it is fully three dimensional. While the peak flux of ions nearly reached the magnetospheric levels, the peak fluxes of energetic electrons were still about a factor of 100 below the magnetospheric level.

The bulk plasma characteristics also changed during the flux transfer event. As seen in Figure 1, the proton density dropped from about 36 cm^{-3} down to about 12 cm^{-3} . Unfortunately, the HAM experiment was passive throughout the flux transfer event and thus an active verification of the number density was not possible. It should be mentioned that there was no evidence of any increase in the double sphere antenna background noise at frequencies above the corresponding plasma frequency (31 kHz), as is normally observed. The proton bulk flow velocity was about 75 km/s, dropped to about 50 km/s, climbed to 150 km/s, and then fluctuated between these two values before returning to its magnetosheath value. In the flux transfer event, the electron

temperature increased to about 5 x 10^5 °K (K. Ogilvie, private communication, 1980).

The abrupt onset and termination of the flux transfer event is also evident in a plot of the current densities shown in Figure 6. Currents were determined by taking the gradient of the magnetic field and calculated current densities were based on the assumption of a constant 20 km/s velocity throughout the structure. This is a somewhat arbitrary assumption, maintained in all cases studied here, and the velocity, which was characteristic of the motion of the current layer per se, may have varied from event to event. This would result in misscaling of the absolute values of the current densities, although the relative currents within each interval should be accurate. The current density increased abruptly at 0212:12 U.T. and fluctuated at high levels until it abruptly dropped to the original magnetosheath levels at 0214:33 U.T. The period of enhanced current fluctuations was simultaneous (to the time resolution of the particle measurements) with the period of enhanced energetic particle observations.

Besides the large scale perturbations of the magnetic field, Figure 5 shows that the magnetic field wave structure was considerably modified. The slow magneto-acoustic waves disappeared near the flux transfer event, and at the center of the flux transfer event there appeared high frequency compressible waves with a period of about 1 s which was very close to the proton cyclotron frequency. To attempt to identify these waves, we did a minimum variance analysis on the waves. These ~1 Hz "waves" within the flux transfer events turned out to be unwavelike in the sense that the field never completed a single full

wave cycle. The cases where nearly a full cycle was completed and where a sense of field rotation could be assigned divided approximately evenly between right and left-handed polarizations. Minimum variance directions were seldom well defined and appeared randomly oriented. The structures were not clearly correlated at the two spacecraft.

Figure 7 shows the power spectrum of the magnetic field waves during the flux transfer event. For comparison, the power spectrum for the magnetosheath period discussed in Section A is also shown. Except for the frequency range of the observed magneto-acoustic waves (.025 Hz to .05 Hz) in the magnetosheath, the power spectral density for the low frequency magnetic waves was greater all across the spectrum in the flux transfer event than in the nominal magnetosheath. From about 0.2 Hz to 3 Hz, the power spectral density in the flux transfer events was typically about an order of magnitude greater than in the nominal magnetosheath.

Figure 8 shows two examples of wideband data acquired during the flux transfer event. It can be seen that the low frequency (< 1 kHz) continuum was significantly more intense during the flux transfer event than in the nominal magnetosheath. In the magnetic spectrum analyzer data, this noise was intense, from 5.6 Hz through 562 Hz, indicating that this component had a substantial electromagnetic component.

The other type of emission continuously present in the nominal magnetosheath, namely the wideband "spikes", also increased in the flux transfer event. The spectrum analyzer data show that the "spikes" did not significantly change their intensity or their frequency range, but rather their frequency of occurrence increased dramatically. In fact,

they occur in such rapid succession that the spectrum analyzer, which has a detector time constant of 50 ms, does not have time to recover completely between spikes. The effect of this is to make it appear in the digital spectrogram as if the low frequency continuum extends to higher frequencies during the flux transfer event. However, it can be seen in the higher time resolution wideband data that the higher frequency data are a series of spikes and not a higher frequency extension of the continuum.

The "festoon-shaped" emissions and the "lion roars" observed in the nominal magnetosheath did not appear during the flux transfer event. This is probably due to the fact that the magneto-acoustic waves, with which these two types of emissions were associated, also did not occur during the FTE.

Electron cyclotron harmonic waves appeared more frequently than in the nominal magnetosheath; and they appeared to be quasi-periodic with a period of about 1.25 seconds as, for example, between 0212 and 0213 U.T. The half-spin period of the spacecraft is 1.52 seconds, so it is unlikely that the observed periodicity is a spin modulation effect. It is more likely that the electron cyclotron harmonics are associated with the ~1 Hz "waves" appearing in the magnetometer data as the "festoon-shaped" emissions were associated with the magneto-acoustic waves in the nominal magnetosheath. In the magnetic spectrum analyzer data, emissions near the electron gyrofrequency were observed simultaneously with intense bursts of electron cyclotron harmonics. In the wideband analog data, these emissions appeared as a narrow line just below the electron gyrofrequency. These magnetic bursts tended to occur near the edge of a flux transfer event or during a passage close

to a flux transfer tube.

Figure 9 shows the spectrum of the electric and magnetic field waves using the same format as Figure 4 for a period which is situated well inside the flux transfer event and which contains an integral number of frequency sweeps of the HAM experiment. Except for the frequency range from a few hundred Hz to about 1 kHz, and then only for the 30 m ISEE 2 antenna, the spectral density was greater in the flux transfer event than in the nominal magnetosheath. The appearance of a broad continuum below 1 kHz with a monotonically increasing spectral density with decreasing frequency is evident. Below 1 kHz, the electric field spectral density measured by the 215 m antenna on ISEE 1 is proportional to f^{-2}. Below 100 Hz the magnetic field spectral density is proportional to $f^{-3.3}$ and between 100 Hz and 562 Hz it is proportional to $f^{-4.7}$.

Between 10 Hz and 3 kHz, the electric field strength as measured by the 30 m dipole antenna was always less than the field strength measured by the 215 m dipole antenna. This apparent discrepancy could be due to the separation of the spacecraft, but we believe this is unlikely. The magnetic field and the plasma parameters measured by both spacecraft were quite similar during this flux transfer event. Later in the pass, in the turbulent region nearer the magnetopause, it is more likely that the spacecraft separation was responsible for differences in plasma waves observed on the two spacecraft. A more likely explanation for the observed differences is that λ_D, the Debye length, in the flux transfer event was larger than normal and comparable to the antenna length on ISEE 2. For $T = 5 \times 10^5$ °K and $N = 12$ cm^{-3}, $\lambda_D = 14$ m, which is nearly equal to the length of each half of the ISEE 2 dipole. Such a long Debye

length was probably shielding the antenna and causing the observed reduced field strengths in the 10 Hz to 3 kHz frequency range.

Figures 5 and 9 indicate that in the frequency range from 562 Hz to 3.1 kHz in the flux transfer event both long and short wavelength effects were observed, while above 3.1 kHz only short wavelength waves were present. The average field strengths at 562 Hz and 1.78 kHz from the 73.5 m and 215 m antennas are nearly the same in Figure 9. And in the GUM-HAM comparison of Figure 5 at different times in the flux transfer event, in the frequency range from 562 Hz to 3.1 kHz, the GUM and HAM field strengths are nearly equal. These observations indicate the presence of waves with wavelengths greater than 215 m. At 1 kHz and 3.1 kHz and above, in Figure 9 the average field strengths measured on the 73.5 m antenna are always larger than the field strengths measured on the 215 m antenna. The GUM-HAM comparison in Figure 5 also shows that at different times in the flux transfer event in the frequency range from 562 Hz to 3.1 kHz, the average field strength measured on the 73.5 m antenna can be up to 20 dB higher than measured on the 215 m antenna. These observations indicate the presence of waves with wavelengths less than 215 m.

At 1 kHz, 3.1 kHz and at 5.6 kHz, the field strengths measured on the 73.5 m double sphere antenna were larger than the field strengths on either the 30 m or 215 m long-wire antennas. We believe this could indicate very short wavelengths, $\lambda < 30$ m. The double sphere antenna is much better able to detect wavelengths shorter than its tip-to-tip separation distance than are the two wire antennas.

From 5.6 kHz to 50 kHz, the electric field strengths were greater as measured on the 30 m and 73.5 m antennas than as measured on the 215

m antenna. This indicates wavelengths between 30 m and 215 m. The enhanced noise at 56 kHz was due to long wavelength Langmuir waves near the local electron plasma frequency.

When the HAM data are plotted as a function of time, it is clear that the signal always has a local minimum when the antenna is perpendicular to the ambient magnetic field. Therefore, the polarization analysis described in section A was applied to the data obtained inside this flux transfer event, and the results are shown in Figure 10. The frequency range used was 1.5 to 42.0 kHz, and again the antenna spin plane was divided into 18 10° angular sectors, measured with respect to the projection of the magnetic field into the spin plane. The dashed curve shows the histogram obtained by using all the points: there is a sharp peak at 145° ± 10°. The ecliptic longitude of the magnetic field varied between about 245° and 270°, so the peak field occurred when the antenna was near ecliptic longitude 45° or 225°, which is again near the direction of flow. These few, very strong signals were eliminated by setting a threshhold of 1 x $10^{-12}v^2m^{-2}Hz^{-1}$, which eliminated only 83 out of 4300 data points. The resulting histogram is also shown in Figure 10 as the continuous curve; the field strength now varies more or less sinusoidally with antenna phase, and exhibits a clear minimum when the antenna is perpendicular to the magnetic field. A similar result, but without the peaks, has also been obtained from the GUM experiment; the maximum field strength in the 10 kHz channel occurs when the Heppner antenna is most nearly parallel to the ambient magnetic field. At the present time, we have not yet been able to determine the polarization at lower frequencies.

A remarkable feature of the HAM data is the amount of frequency structure which appears in the data. Of course, with a swept-frequency receiver, frequency structure, temporal structure and spacecraft spin modulation are all convolved together. To test whether there are any spectral features related to the electron cyclotron frequency or its harmonics, the HAM spectra were re-plotted after normalization of each frequency step to the measured cyclotron frequency. No additional order appeared in the spectra, from which we conclude that the bursty nature of the HAM spectra is not related to any cyclotron harmonic structure.

After this first flux transfer event, the spacecraft re-entered the nominal magnetosheath , which we have described in Section A. Between 0228:50 and 0230:30 U.T., there was a strange event identified in the magnetic field data when the field became steady (at a value near the peak value in the magneto-acoustic wave) except for the appearance of weak compressible waves of frequency ~1 Hz. Plasma wave features observed during this time interval included sporadic "festoon-shaped" emissions and sporadic electron cyclotron harmonics. These waves are indicative respectively of the nominal magnetosheath and the flux transfer event. In the magnetic data, emissions near the electron cyclotron frequency are seen, as they were just before and just after the flux transfer event. The magnetic field did not undergo the positive B_N to zero excursion representative of a flux transfer event. This event was probably not a flux transfer event, but may have been an oblique passage through or near a flux transfer event tube.

The second flux transfer event is illustrated in Figure 11 and is quite similar to the first. The "lion roars" and "festoon-shaped"

emissions which are characteristic of the nominal magnetosheath cease about 0232:30 and do not reappear until 0237:55 U.T. The dominant plasma wave features are again electron cyclotron harmonics and much "spiky turbulence". The electron cyclotron turbulence is well correlated with the ~1 Hz magnetic field fluctuations, which are also present in the flux transfer event. Unlike the first flux transfer event, the magneto-acoustic wave with a period of ~40 s is evident throughout most of the second flux transfer event. However, the "lion roars" occur only before and after the flux transfer event when the magnetic field magnitude is sufficiently low and β is sufficiently high.

The B_N component of the magnetic field changed less during the second FTE than during the first, and there was a corresponding decrease in the electric field amplitudes (except below 100 Hz on ISEE 2, which is probably a solar array interference effect). Both could be a result of decreased current densities which are displayed in Figure 12. The HAM electric field again has some strong peaks when the antenna lies nearly parallel to the plasma flow direction, superimposed on a weaker background polarized parallel to the local magnetic field.

As shown in Figure 1, increased fluxes of energetic ions and electrons occurred during the second flux transfer event. The peak intensities reached levels slightly lower than those reached during the first flux transfer event. The bulk plasma characteristics changed in similar fashion as they had during the first event; the number density dropped and the proton bulk flow speed dropped, rose and fluctuated.

The HAD propagation experiment was active for 32s starting at 0234:43 U.T. and indicated that the density fluctuated around either 16

or 31 cm^{-3} (the difference being due to the 2π uncertainty in the phase measurements, Harvey et al, 1978). The wave data indicate that 31 cm^{-3} is, in fact, the appropriate value.

C. Turbulent Region

Following the second flux transfer event, the ISEE 1 spacecraft entered the magnetosheath again; from 0238:30 to 0239:50 U.T. all the characteristic plasma wave features described in section A were observed. After this time, the spacecraft entered a highly turbulent region as shown in Figure 13. The characteristic magneto-acoustic waves of the nominal magnetosheath were replaced by very jagged and highly compressional changes of the magnetic field, with all three components of B often changing sense. Compressible waves with period of the order of 1 s appeared. Above 0.5 Hz, the magnetic field power spectra resembled a flux transfer event. Below 0.5 Hz, the magnetic field power spectra resembled the nominal magnetosheath. We feel that this region is insufficiently well understood to attempt as detailed analysis as done for the other regions. Nevertheless, it is possible to delineate five regions illustrated in Figures 14 and 15 with broadly differing characteristics, as follows:

1) 0239:50 -0241:00 U.T. This region had the characteristics of a short flux transfer event. B_N went positive and then negative. The dominant plasma waves present were electron cyclotron harmonics and "spiky" turbulence. The low frequency electromagnetic continuum began to increase about 0240:20 U.T. The plasma wave spectrum resembled a flux transfer event spectrum more than a magnetosheath spectrum. It was elevated above the magnetosheath spectrum at all frequencies except

at the gyrofrequency. Below 1 kHz, the spectrum was from equal to about 5 dB below the second flux transfer event. Between 1 kHz and 10 kHz, it was equal to the second flux transfer event, and at above 10 kHz, the spectrum was equal to the first flux transfer event.

2) 0241:00 to 0242:30 U.T. This region had very little electric field activity except for the very low frequency continuum. In particular, the "spikes" evident nearly continuously in the flux transfer events were reduced to about the frequency of occurrence in the nominal magnetosheath discussed in Section A. However, the spectra for this time period had the same shape as for the two flux transfer events, except it was about 10 dB below the first and 5 dB below the second for all frequencies below the electron plasma frequency.

3) 0242:30 to 0244:20 U.T. In this region, the L-component of the magnetic field was consistently southwards. Both electron cyclotron harmonics (including an intense fundmental) and spikes are evident in the wideband analog data shown in Figure 14c. The wideband data show a clear anti-correlation between the cyclotron harmonics and the spikes, with a periodicity of about 10 s. Examination of Figures 13 and 14c shows that the spikes are correlated with fluctuations of the L-component of the magnetic field. The spikes occurred when B_L was most negative; that is, since $B_N \sim 0$ and the sheath field was more or less parallel to the magnetopause boundary, the spikes occurred when the magnetic field was most nearly aligned parallel to the local solar magnetospheric meridian plane. Below 300 Hz, the spectrum was the same as for the previous few minutes. Above 300 Hz, the large contribution from the electron cyclotron harmonics raised the level to equal or greater than that in the first flux transfer event. Around 56 kHz, very intense emissions

near the electron plasma frequency were evident.

4) 0244:20 to 0248:20. In this region, B_L was northwards. The plasma wave data indicated a mixture of phenomena having traits of both the magnetosheath and of flux transfer events. Enhanced low frequency electromagnetic continuum, electron cyclotron harmonics and frequency of occurrence of spikes all resembled flux transfer events. However, occasional bursts of "lion roars" indicated a magnetosheath-like region.

5) 0248:20 to 0249:20. In this period, B_L was consistently northward and, as can be seen in Figure 1, there was simultaneously a very high plasma flow speed. At this time, the energetic particle intensities began to rise. The spectrum from this time period is very similar to the two main flux transfer events we have examined in section B. This may be associated with the northward direction of B_L, as was the case for the two flux transfer events.

D. Current Layer

Figure 16 shows 4 1/2 minutes of data immediately following the turbulent period discussed in section C. For the first 10 s, the spacecraft was still in the turbulent region. Large gradients were then observed in the magnetic field data. The magnetic field data indicate a flux transfer event of brief duration, from 0249:57 to 0250:08. As shown by the gradients of the magnetic field, the last major current layer was crossed between 0250:23 and 0250:33 U.T. In the magnetic spectrum analyzer data, the low frequency electromagnetic continuum stopped abruptly at 0250:32 U.T.

The plasma wave wideband analog data in Figure 17 show that the current layer resembles a flux transfer event. Electron cyclotron

harmonics, enhanced low frequency continuum and spikes were all present. The magnetic spectrum analyzer data showed enhanced low frequency electromagnetic continuum and some higher frequency magnetic noise bursts.

We can obtain a profile of the drop in electron density by assuming that the magnetospheric continuum radiation has a lower cutoff at the electron plasma frequency. The electric spectrum analyzer data thus shows that the electron plasma frequency dropped abruptly from 31 kHz ($N_e \sim 12$ cm^{-3}) at 0250:30 to 17.8 kHz ($N_e \sim 4$ cm^{-3}) at 0250:30.8 and to 10 kHz ($N_e \sim 1$ cm^{-3}) at 0250:31.5 U.T. These observations are in good agreement with the number density changes shown in Figure 1 and show that the density gradient occurs at the inner edge of the current layer.

E. Outer Magnetosphere

All the plasma wave data changed dramatically betwen 0250:31 and 0250:32 U.T. as the spacecraft crossed the magnetopause into the outer magnetosphere. The low frequency electromagnetic continuum immediately dropped in intensity as shown in the upper panels of Figure 16. The wideband analog data in Figure 17 show that the high frequency continuum radiation dropped in frequency and had a lower cutoff at about 9 kHz at 0251 U. T. No spikes were evident in the electric field data.

From 0251:30 to 0254:40 the most intense high frequency electric field event of the whole magnetosheath to magnetosphere passage occurred. The predominant emission in the electric field data for the first minute was a narrow $(n + 1/2)\ f_g^-$ emission just below the plasma frequency. The electron gyrofrequency was approximately 1.5 kHz. Additional narrowband emissions were present but did not become intense until about 0252:50 U. T.

The wideband analog data in Figure 17 show that emissions were made of several quasimonochromatic tones. The lowest one at a frequency of about 1 kHz had a magnetic component and was probably propagating in the whistler mode. At this frequency, dayside chorus is usually observed in the outer magnetosphere (Tsurutani and Smith, 1977). Going up in frequency, a series of regularly spaced tones were observed between approximately 2 kHz and 7 kHz which are the $(n + 1/2)\ f_g^-$ emissions observed in the magnetosphere usually below the plasma frequency on OGO-5 (Kennel et al., 1970), IMP-6 (Shaw and Gurnett, 1975), S^3-A (Anderson and Maeda, 1977), Hawkeye (Kurth et al., 1979a), GEOS-1 (Christiansen et al., 1978a, b) and ISEE (Gurnett et al., 1979a; Kurth et al, 1979b). Then a line was observed at about 8 kHz which was closer to the line immediately below it than were the preceding ones: this is the noise at the upper hybrid resonance frequency ($f_{UHR} = (f_p^{-2} + f_g^{-2})^{1/2}$) usually seen in the magnetosphere (Christiansen et al.; 1978a, b; Gurnett et al., 1979a; Kurth et al., 1979a, b). The noise seen above this line is probably made of emissions at the f_q frequencies which are persistently seen in the magnetosphere at very low intensities (Christiansen et al. 1978a, b). Low frequency ($f < 300$ Hz) electromagnetic whistler-mode chorus was evident in both the wideband data and the magnetic spectrum analyzer data throughout the outer magnetosphere passage. This low frequency chorus is also typical of the dayside outer magnetosphere. Anderson and Maeda (1977) have shown that the chorus and $(n + 1/2)\ f_g^-$ emissions are produced by low energy electrons which penetrate the dusk-midnight sector of the magnetosphere during geomagnetic storms and then drift eastward through dawn into the dayside outer magnetosphere.

The electric and magnetic field power spectra for this passage in the outer magnetosphere are shown in Figure 18. The contributions from the low and high frequency chorus and from the $(n + 1/2)\ f_g^-$ emissions are intense. The peaks at 10 kHz in the electric field data are near the local electron plasma frequency. Below this frequency, the GUM, GUD and HAM receiver measurements are not significantly different, which indicates wavelengths greater than 215 m. At 17.8 kHz, GUD and HAM agree and are about 15 dB above GUM, which indicates a wavelength between 30 and 215 m. At 31 kHz HAM is about 15dB above GUD, which is in turn about 15 dB above GUM; this indicates wavelengths less than 30 m. Even at 50 kHz, HAM still measured a strong signal. While the phenomena observed below 10 kHz are very common in the magnetosphere, the strong high frequency short wavelength signals are not commonly observed throughout the outer magnetosphere.

F. Boundary Layer

From 0254:37 to 0257:46 U. T. the spacecraft was not in the outer magnetosphere but rather in a region we identify as the boundary layer. As shown in Figure 1, the number density increased and the bulk plasma flow speed increased. As can be seen in Figures 19 and 20, the plasma wave observations are nearly identical to our observations in the flux transfer events and in the magnetopause current layer. Spikes occurring very frequently and electron cyclotron harmonics are the dominant features in the electric field data. On the magnetic spectrum analyzer data, strong low frequency electromagnetic continuum radiation was again present. The electric and magnetic field power spectra shown

in Figure 21 show the close similarity between the boundary layer plasma wave phenomena and those in the flux transfer events and the magnetopause current layer.

ISEE 1 reentered the outer magnetosphere at 0257:46. At three additional times it had brief encounters with flux transfer events or boundary layer conditions: 0300:15 U. T., 0302:30 U. T. and 0309:10 U. T. However, each event lasted less than 15 seconds, which is not sufficient to allow the analysis carried out for the earlier events.

V. DISCUSSION AND SUMMARY

A. The Nominal Magnetosheath

For the pass that we have studied, the magnetic field in the magnetosheath fluctuated at an ultra-low frequency with a period of 20-40 s out of phase with the simultaneously occurring density fluctuations. Tsurutani et al. (1981b) have identified these fluctuations as slow-mode magneto-acoustic waves propagating nearly perpendicular to the ambient magnetosheath magnetic field. Two types of plasma wave emissions characteristic of the nominal magnetosheath were found to be associated with these magneto-acoustic waves: "lion roars" and "festoon-shaped" emissions. The whistler-mode "lion roars" occur in the high β (low $|B|$) phase of the waves and have been shown by Tsurutani et al. (1981b) to be generated by an electron cyclotron instability driven by a temperature anisotropy. The "festoon-shaped" emissions occur in the low β (high $|B|$) phase of the waves and are electrostatic. The polarization of the "festoon-shaped" emissions changes with frequency. The higher frequency ($\sim$ 2kHz) portion of the emissions is enhanced perpendicular to the ambient magnetic field while the lower frequency portion is enhanced more nearly parallel to the ambient magnetic field. A comparison of the signals on the three antennas for periods when the "festoon-shaped" emissions are present indicate wavelengths less than 73 m but greater than 30 m. We have not been able to identify the mode or the instability which produces these "festoon-shaped" emissions.

Three plasma wave emissions characteristic of the nominal magnetosheath but not associated with the magneto-acoustic waves have

also been identified: a very low frequency continuum, spikes, and bursts of electron cyclotron harmonics. The very low frequency continuum is always present. It is electromagnetic, but a comparison of the magnetic to electric intensities is not useful for determining the mode because of the unknown contribution to the electric spectrum from the solar array interference. The high noise levels at low frequencies due to the solar array interference also make wavelength measurements impossible.

The spikes represent the main contribution to the magnetosheath spectrum between the ion and electron plasma frequencies. They are predominantly electrostatic except that bursts of magnetic noise near the electron gyrofrequency are observed accompanying the most intense spikes. Higher electric field strengths are observed on the shorter antennas indicating wavelengths less than 215 m. The most intense spikes are polarized in the direction of the plasma flow. The remainder are polarized parallel to the ambient magnetic field. The spikes are very brief ($\tau < 8$ ms) and occur simultaneously across the spectrum to the time resolution of the spectrum analyzers. It is very difficult to explain the wide frequency range and brief time duration in terms of known waves. The spikes have the characteristics of small scale plasma potential irregularities convecting past the antenna. This could explain the alignment with the plasma flow and why the field strengths measured by HAM were greater than those measured by GUM or GUD. The Mozer antenna measures the potential difference between two points while the long wire antennas measure the average over the length of the elements, the Mozer antenna is more sensitive to extremely short wavelengths or small-scale irregularities. In future research we will

study the nature of these fluctuations further by analyzing the response of the different antennas to varying plasma potential irregularities.

The electrostatic electron cyclotron harmonics occur rarely and briefly in the magnetosheath. They do not appear correlated with any magnetic field fluctuations, changes in particle intensities or changes in plasma parameters that we are capable of observing. While the $nf_{\overline{g}}$ resonance frequencies are easily observed by active sounding experiments, they are unexpected as naturally occurring waves because of their relatively high damping for all propagation directions except exactly perpendicular to the ambient magnetic field [Christiansen, et al., 1978a, b]. In the magnetosheath these emissions are too brief to make any wavelength comparisons.

B. Flux Transfer Events

In addition to the large positive B_N excursion followed by a large negative B_N excursion and then return to zero that identifies a flux transfer event, we have observed other magnetic field, plasma, energetic particle and plasma wave characteristics common to flux transfer events. We observed large increases in current densities simultaneous with the periods of enhanced energetic particle observations. In the flux transfer events we observed compressible magnetic fluctuations with a frequency of ~ 1 Hz which is near the ion cyclotron frequency. We could not identify a mode for these fluctuations because sometimes they exhibited left-handed polarization and sometimes they exhibited right-handed polarization. The power spectral density of the low frequency magnetic fluctuations was greater all across the spectrum (except for the .025 Hz to .05 Hz range of the magnetosheath magneto-acoustic waves) in the flux transfer events as compared to the nominal magnetosheath.

And in the frequency range 0.2 Hz to 3 Hz, the power spectral density in the flux transfer event was about an order of magnitude greater than in the nominal magnetosheath.

The main plasma wave phenomena observed during flux transfer events are a low frequency continuum, "spikes" and electron cyclotron harmonics. The low frequency continuum (< 1 kHz) is more intense during the flux transfer event than in the nominal magnetosheath and it has a substantial electromagnetic component. Antenna comparison measurements indicate the low frequency continuum has wavelengths greater than 215 m. The increase in the intensity of the low frequency continuum during flux transfer events could be due to the increase in energetic particle fluxes or the increased current densities.

The "spikes" increase dramatically in the flux transfer event. They do not significantly change their intensity or their frequency range, but rather their frequency of occurrence increases substantially. They occur so frequently that in the spectrum analyzer data they appear as a high frequency continuum. If, as we have suggested, the "spikes" are a result of plasma potential irregularities convecting past the spacecraft, the increased frequency of occurrence could be due to the higher flow velocities present in the flux transfer events. As in the nominal magnetosheath, we found that the "spikes" have wavelengths less than 215 m, the most intense "spikes" are polarized in the direction of the plasma flow and the remainder are polarized parallel to the ambient magnetic field.

Electron cyclotron harmonic waves appear more frequently in flux transfer events than in the nominal magnetosheath. They appear at times to be quasi-periodically related to the magnetic fluctuations near the

ion-cyclotron frequency. This relationship is similar to that between the "festoon-shaped" emissions and the magneto-acoustic waves in the nominal magnetosheath. Electromagnetic emissions near the electron gyrofrequency occur simultaneously with intense bursts of electron cyclotron harmonics near the edge of flux transfer events. The presence of both long and short wavelength effects in the frequency range from 562 Hz to 3.1 kHz makes it difficult to unscramble the waves. However, the most plausible explanation is that the long wavelength observations correspond to the electromagnetic bursts while the very short wavelengths correspond to the electrostatic electron cyclotron harmonics. At this time, we do not know whether the increased current densities, energetic particles, flow velocities, or some combination of the above are responsible for the enhanced wave intensities near the electron gyrofrequency and its harmonics.

During the flux transfer events, long wavelength Langmuir waves have spectral densities about 10 dB higher than in the nominal magnetosheath. This is most likely due to the enhanced energetic electron population observed in the flux transfer events [Anderson et al, 1981].

C. Turbulent Region

In the turbulent region the magnetic field above 0.5 Hz was dominated by jagged and highly compressional fluctuations with a period of about 1 s. Based on the changes in B_N and the characteristics of the plasma waves present, the turbulent region appeared to consist of many brief flux transfer events separated by regions of magnetosheath. For much of the time the spectra closely resembled the spectra in flux transfer events. Enhanced low frequency continuum, "spikes", and electron cyclotron harmonics were usually present. When B_L was southward, the electron cyclotron harmonics and the "spikes" were

anti-correlated and quasiperiodic with a period of about 10 s. The "spikes" occurred when B_L was most negative and thus most nearly aligned to the local solar magnetospheric meridian plane. Conditions were changing too fast in this region to make any comparisons between spacecraft or between HAM and GUM.

D. Current Layer

The plasma waves observed in the current layer were the same as those characteristic of the flux transfer events, namely electron cyclotron harmonics, enhanced low frequency continuum and "spiky" turbulence. The density gradient at the magnetopause was observed at the inner edge of the current layer.

E. Outer Magnetosphere

In the outer magnetosphere we observed the characteristic $(n + 1/2)$ f_g emissions, whistler-mode chorus and upper hybrid resonance emissions. Strong naturally occurring short wave-length emissions at the f_q frequencies were also observed. Such an observation is unusual, for they are normally seen at such intensities only when stimulated by active experiments. The observation of the rare f_q resonances is probably related to the close proximity of the magnetopause.

F. Boundary Layer

The plasma wave observations in the boundary layer were nearly identical to those in flux transfer events and in the magnetopause current layer. The dominant plasma waves are enhanced frequency of occurrence of "spikes", strong low frequency electromagnetic continuum and electron cyclotron harmonic emissions. The electric and magnetic field power spectra in the boundary layer are nearly identical to those in the flux transfer events and the magnetopause current layer.

VI. CONCLUSIONS

In this paper we have shown that the magnetosheath, flux transfer events, the magnetopause current layer, the outer magnetosphere and the boundary layer can be identified by their magnetic field and plasma wave characteristics as well as by their plasma and energetic particle signatures. The plasma wave characteristics of the flux transfer events, magnetopause current layer and the boundary layer are nearly identical and these regions are separated out only by their positions relative to the outer magnetosphere. In the magnetosheath we have found that "lion roars" and "festoon-shaped" emissions are related to ultra-low-frequency magnetic field fluctuations. Where possible, we have identified the wavelengths and polarizations of the plasma waves in the various regions. To better understand some of the wave observations we will do a future theoretical study of the response of the various antennas to plasma potential irregularities convecting past the spacecraft and the response of the antennas to different wavelengths and frequencies when the Debye length is comparable to the antenna length. One point is very obvious from our research: in regions of space where conditions are changing very rapidly, one needs high time resolution measurements simultaneously from several antennas of significantly different lengths on the same spacecraft.

ACKNOWLEDGEMENTS

We wish to thank D. A. Gurnett, C. T. Russell, L. A. Frank, G. Paschmann, S. J. Bame and K. W. Ogilvie for the use of their ISEE data. This research was supported at the University of Iowa by NASA contracts NAS5-20093 and NAS5-20094 and by the Office of Naval Research; at the University of California at Los Angeles by NASA contract NAS5-25722; at the Jet Propulsion Laboratory, California Institute of Technology by NASA contract NAS 7-100, and at the Observatoire de Paris by the Centre National d'Etudes Spatiales under contracts *nos.* SL.180.01.E and CNES/214.

REFERENCES

Anderson, R. R, G. K. Parks, T. E. Eastman, D. A. Gurnett and L. A. Frank, "Plasma Waves Associated With Energetic Particles Streaming Into the Solar Wind From the Earth's Bow Shock," accepted for publication, J. Geophys. Res., 1981.

Anderson, Roger R. and Kaichi Maeda, "VLF Emissions Associated With Enhanced Magnetospheric Electrons," J. Geophys. Res., 82, 135, 1977.

Christiansen, P., P. Gough, G. Martelli, J. J. Bloch, N. Cornilleau, J. Etcheto, R. Gendrin, D. Jones, C. Beghin and P. Decreau, "Geos I: Identification of Natural Magnetospheric Emissions," Nature, 272, 682, 1978a.

Christiansen, P. J., M. P. Gough, G. Martelli, J. J. Bloch, N. Cornilleau, J. Etcheto, R. Gendrin, C. Beghin, P. Decreau and D. Jones, "Geos-1 Observations of Electrostatic Waves, and Their Relationship with Plasma Parameters," Space Sci. Rev., 22, 383, 1978b.

Elphic, R. C. and C. T. Russell, "ISEE-1 and 2 Magnetometer Observations of the Magnetopause," Magnetospheric Boundary Layers, ESTEC, Noordwijk, The Netherlands, 43, 1979.

Frank, L. A., K. L. Ackerson, R. J. DeCoster, and B. G. Burek, "Three-Dimensional Plasma Measurements Within the Earth's Magnetosphere," Space Sci. Rev., 22, 739, 1978.

Gurnett, D. A., F. L. Scarf, R. W. Fredricks and E. J. Smith, "The ISEE-1 and ISEE-2 Plasma Wave Investigation," IEEE Trans. Geosci. Electr., GE-16, 225, 1978.

Gurnett, D. A., R. R. Anderson, F. L. Scarf, R. W. Fredricks and E. J. Smith, "Initial Results From the ISEE-1 and -2 Plasma Wave Investigation, Space Sci. Rev., 23, 103, 1979a.

Gurnett, D. A., R. R. Anderson, B. T. Tsurutani, E. J. Smith, G. Paschmann, G. Haerendel, S. J. Bame, and C. T. Russell, "Plasma Wave Turbulence at the Magnetopause: Observations from ISEE 1 and 2," J. Geophys. Res., 84, 7043, 1979b.

Harvey, C. C., J. Etcheto, Y. DeJavel, R. Manning and M. Petit, "The ISEE Electron Density Experiment," IEEE Trans. Geosci. Electr., GE-16, 231, 1978.

Harvey, C. C., J. Etcheto, and A. Mangeney, "Early Results From the ISEE Electron Density Experiment," Space Sci. Rev., 23, 39, 1979.

Kennel, C. F., F. L. Scarf, R. W. Fredricks, J. H. McGehee, and F. V. Coroniti, "VLF Electric Field Observations in the Magnetosphere," J. Geophys. Res., 75, 6136, 1970.

Kurth, W. S., M. Ashour-Abdalla, L. A. Frank, C. F. Kennel, D. A. Gurnett, D. D. Sentman and B. G. Burek, "A Comparison of Intense Electrostatic Waves Near f_{UHR} With Linear Instability Theory," Geophys. Res. Letts., 6, 487, 1979a.

Kurth, W. S., J. D. Craven, L. A. Frank and D. A. Gurnett, "Intense Electrostatic Waves Near the Upper Hybrid Resonance Frequency, J. Geophys. Res., 84, 4145, 1979b.

Ogilvie, K. W. and J. D. Scudder, "First Results From the Six-Axis Electron Spectrometer on ISEE-1," Space Sci. Rev., 23, 123, 1979.

Parks, G. K., C. S. Lin, K. A. Anderson, R. P. Lin, H. Reme, F. Coroniti, C. Meng and R. Pellat, "Particle Boundary Structures at the Magnetopause and the Plasma Sheet," Magnetospheric Boundary Layers, ESTEC, Noordwijk, The Netherlands, 151, 1979.

Parks, G. K., H. Reme, A. Saint-Marc, C. S. Lin, R. P. Lin and K. A. Anderson, "ISEE 1/2 Timing of Transient Particle Fluxes in the Vicinity of and Beyond the Magnetopause," J. Geophys. Res., this issue, 1981.

Paschmann, G., N. Sckopke, G. Haerendel, J. Papamastorakis, S. J. Bame, J. R. Asbridge, J. T. Gosling, E. W. Hones, Jr., and E. R. Tech, "ISEE Plasma Observations Near the Subsolar Magnetopause," Space Sci. Rev., 22, 717, 1978.

Paschmann, G., "Plasma Structure of the Magnetopause and Boundary Layer," Magnetospheric Boundary Layers, ESTEC, Noordwijk, The Netherlands, 25, 1979.

Rodriguez, Paul, "Magnetosheath Electrostatic Turbulence," J. Geophys. Res., 84, 917, 1979.

Russell, C. T., "The ISEE 1 and 2 Fluxgate Magnetometers," IEEE Trans. Geosci. Electr., GE-16, 239, 1978.

Russell, C. T. and R. C. Elphic, "Initial ISEE Magnetometer Results: Magnetopause Observations," Space Sci. Rev., 22, 681, 1978.

Shaw, Robert R. and Donald A. Gurnett, "Electrostatic Noise Bands Associated With the Electron Gyrofrequency and Plasma Frequency in the Outer Magnetosphere," J. Geophys. Res., 80, 4259, 1975.

Siscoe, G. L., L. Davis, Jr., P. J. Coleman, Jr., E. J. Smith and D. E. Jones, "Shock-Aligned Magnetic Oscillations in the Magnetosheath: Mariner 4," J. Geophys. Res., 72, 5524, 1967.

Smith, E. J., R. E. Holzer, and C. T. Russell, "Magnetic Emissions in the Magnetosheath at Frequencies Near 100 Hz," J. Geophys. Res., 74, 3027, 1969.

Smith, Edward J. and Bruce T. Tsurutani, "Magnetosheath Lion Roars," J. Geophys. Res., 81, 2261, 1976.

Tsurutani, Bruce T. and Edward J. Smith, "Two Types of Magnetospheric ELF Chorus and Their Substorm Dependences," J. Geophys. Res., 82, 5112, 1977.

Tsurutani, B. T., E. J. Smith, R. M. Thorne, R. R. Anderson, D. A. Gurnett, G. K. Parks, C. S. Lin and C. T. Russell, "Wave-Particle Interactions at the Magnetopause: Contributions to the Dayside Aurora," Geophys. Res. Letts., 8, 183, 1981a.

Tsurutani, B. T., E. J. Smith, C. T. Russell, R. R. Anderson, K. W. Ogilvie, J. D. Scudder, D. N. Baker and E. W. Jones, Jr., "Lion Roars and Slow Mode Hydromagnetic Waves in the Magnetosheath," J. Geophys. Res., this issue, 1981b.

FIGURE CAPTIONS

FIGURE 1 Magnetic field and plasma parameters observed on ISEE 1 from 02:02 to 03:10 U.T. on November 8, 1977. The top three panels show the magnetic field in boundary normal coordinates which are described in the text. Panel 4 contains the magnitude of the magnetic field. Panels 5 and 6 contain the two-dimensional proton number density and velocity courtesy of G. Paschmann. Panels 7 and 8 show the intensities of energetic ions and electrons. The regions we examine in detail in this paper are indicated at the top.

FIGURE 2 Data from the nominal magnetosheath. The top panels show the GUM electric and magnetic spectrum analyzer data. All data points are shown and each panel covers 60 dB in dynamic range. The baselines for each panel are the GUM electric and magnetic receiver noise levels shown in Figure 4. The data gap in the electric spectrum analyzer data is due to the HAM experiment being active for 32 s. The data gaps at mid-frequency in the magnetic spectrum analyzer data are from interference from the scan platform. The middle panel shows the magnitude of the magnetic field measured by the RUM experiment. The last eight panels show the outputs from the GUM and HAM receivers, after processing as described in Section 3 to give a point every 16 s at each frequency. In these panels the

dynamic range is 60 dB, the baseline is the GUM noise level and the horizontal dotted line is the HAM noise level. The GUM and HAM points are joined respectively by solid and dotted lines. The contribution to the spectrum analyzer data of the low frequency continuum, spikes, "festoon-shaped" emissions and the "lion roars" are pointed out.

FIGURE 3 Electric field wideband analog data in the nominal magnetosheath from 0224 to 0229 U.T. The upper panel for each set is 0-1 kHz and the second panel is 0-10 kHz. For reference, the magnitude of the magnetic field is included in the bottom panel. Note that the "lion roars" occur in the low |B| phase and the "festoon-shaped" emissions occur in the high |B| phase of the magnetic waves.

FIGURE 4 The minimum, mean and average power spectrum seen in the nominal magnetosheath by GUM, GUD and HAM. The period covered is from 0226:43 to 0228:51. The vertical bars represent the minimum and maximum values measured by GUM and GUD, and the horizontal ticks indicate the mean electric field: GUM and GUD are respectively on the left and right of each pair of bars. The mean (solid line) minimum and maximum (dotted lines) field strengths measured by HAM are plotted betwen 469 Hz and 50.6 kHz. The three antenna

plus receiver noise spectra are also shown. Above these electric field spectra the GUM magnetic field power spectrum multiplied by c^2 is plotted on the same axes, offset by a factor of 10^3 to avoid confusion.

FIGURE 5 Data from a flux transfer event. Same description as for Figure 2 except the 3 components of the magnetic field in boundary normal coordinates have been added. In the electric field data, the low frequency continuum increases in intensity and electron cyclotron harmonics and spikes occur more frequently. In the magnetic spectrum analyzer data the low frequency emissions increase abruptly during the flux transfer event. Bursts of magnetic noise near the electron gyrofrequency are evident near the edges of the flux transfer event.

FIGURE 6 Parallel and perpendicular current densities determined for the first flux transfer event shown in Figure 5. As discussed in the text, a boundary motion velocity of 20 km/s was assumed in this determination. The enhanced current densities during the flux transfer event are quite evident.

FIGURE 7 Power spectra of the low frequency magnetic field waves observed during the flux transfer event and in the nominal magneto-sheath. Except for the frequency range of the magnetic-acoustic waves (.025-.05 Hz) in the magnetosheath the power spectral density for the low

frequency magnetic waves is greater all across the frequency spectrum in the flux transfer event than in the nominal magnetosheath.

FIGURE 8 Wideband analog data from the flux transfer event. The inreased frequency of occurrence of the spikes and electron cyclotron harmonics and the increased low frequency continuum are evident. No "lion roars" or "festoon-shaped" emissions are observed.

FIGURE 9 Power spectra of the plasma wave electric and magnetic field data for the flux transfer event shown in Figure 5.

FIGURE 10 Histograms of the mean HAM electric field strength in the frequency range 1.5 to 42.2 kHz as a function of the antenna phase angle in the first flux transfer event. The antenna phase is measured with respect to the projection of the (high resolution) magnetic field onto the spin plane, and the data interval is 0212:36 to 0214:11. The dashed line was obtained using all data points, and the continuous line after elimination of the 83 points (out of 4300) which had a field strength greater than 1×10^{-12} $V^2m^{-2}Hz^{-1}$. This latter curve has been plotted after multiplying the values by a factor of 5.

FIGURE 11 Data from the second flux transfer event.

FIGURE 12 Parallel and perpendicular current densities determined for the second flux transfer event shown in Figure 11. A flow speed of 20 km/s was also assumed in this determination. Again enhanced current densities are observed during the flux transfer event, but they are lower than those observed during the first flux transfer event.

FIGURE 13 Magnetic field data in boundary normal coordinates for the turbulent region.

FIGURE 14 Five selected one-minute examples of electric field wideband analog data in the turbulent region.

FIGURE 15 The average power spectra measured by the GUM experiment during five intervals in the turbulent region: ..... 0239:50 to 0241:00, ...0241:00 to 0242:00, ...0242:30 to 0244:20, ...0244:20 to 0248:20, and 0248:20 to 0249:20. The spectra in the two flux transfer events and in the nominal magnetosheath are drawn for comparison (solid lines).

FIGURE 16 Data from the current layer region, magnetopause and outer magnetosphere. The last current layer was crossed by 0250:31 U. T.

FIGURE 17 Electric field wideband analog data from the current layer region, magnetopause and outer magnetosphere.

FIGURE 18 Power spectra of the plasma wave electric and magnetic field data for the outer magnetosphere from 0252 to 0254 U. T.

FIGURE 19 Data from the boundary layer. Same description as for Figure 5.

FIGURE 20 Wideband analog data showing entry into and exit from the boundary layer.

FIGURE 21 Power spectra of the plasma wave electric and magnetic field data for the boundary layer region from 0255 to 0257 U. T.

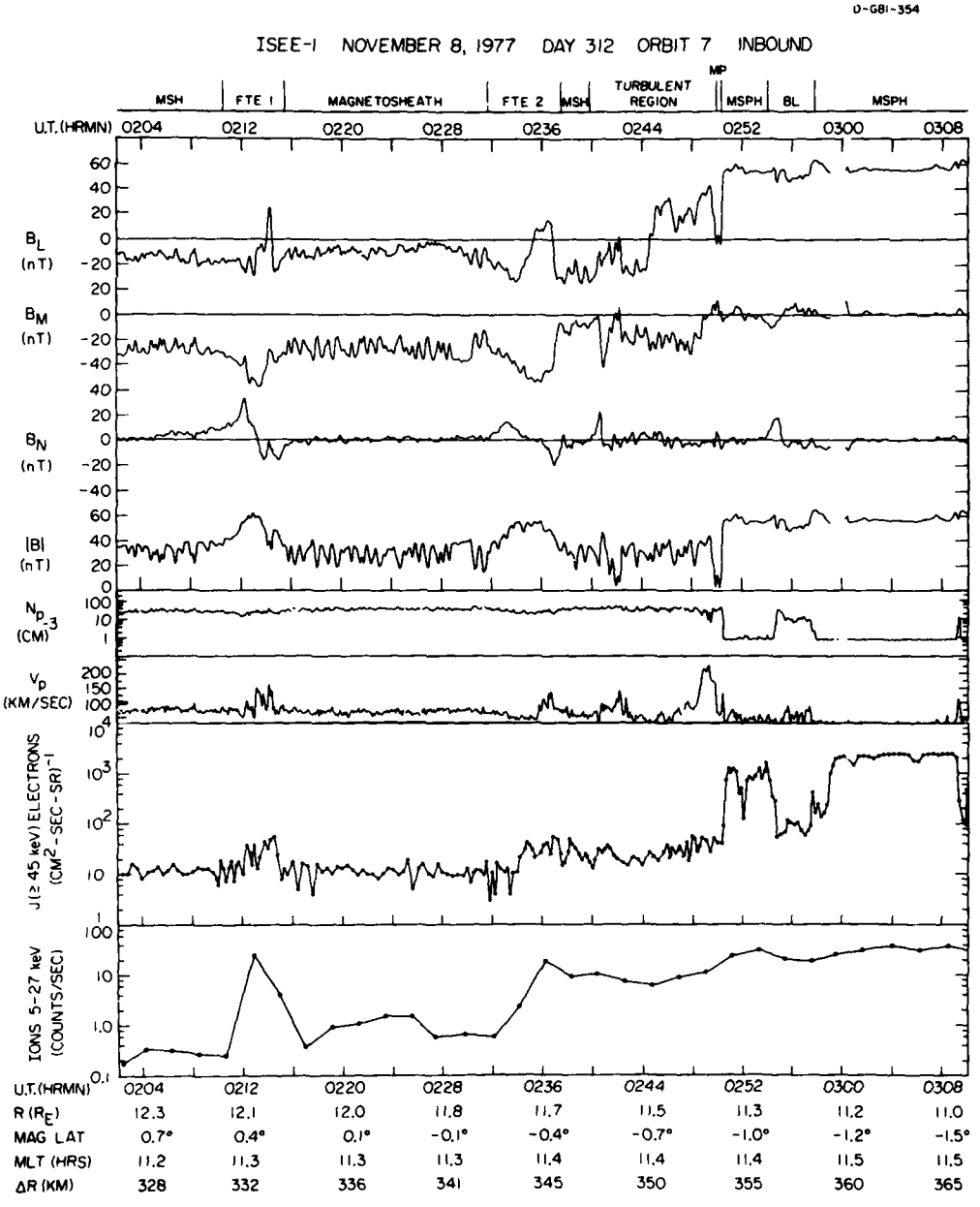
D-G81-354
ISEE-1 NOVEMBER 8, 1977 DAY 312 ORBIT 7 INBOUND
MSH
FTE 1
MAGNETOSHEATH
FTE 2
MSH
TURBULENT REGION
MP
MSPH
BL
MSPH
U.T.(HRMN) 0204 0212 0220 0228 0236 0244 0252 0300 0308
B_L (nT)
B_M (nT)
B_N (nT)
|B| (nT)
N_p (CM^-3)
V_p (KM/SEC)
J(≥ 45 keV) ELECTRONS (CM^2-SEC-SR)^-1
IONS 5-27 keV (COUNTS/SEC)
U.T.(HRMN) 0204 0212 0220 0228 0236 0244 0252 0300 0308
R (R_E) 12.3 12.1 12.0 11.8 11.7 11.5 11.3 11.2 11.0
MAG LAT 0.7° 0.4° 0.1° -0.1° -0.4° -0.7° -1.0° -1.2° -1.5°
MLT (HRS) 11.2 11.3 11.3 11.3 11.4 11.4 11.4 11.5 11.5
ΔR (KM) 328 332 336 341 345 350 355 360 365

Figure 1

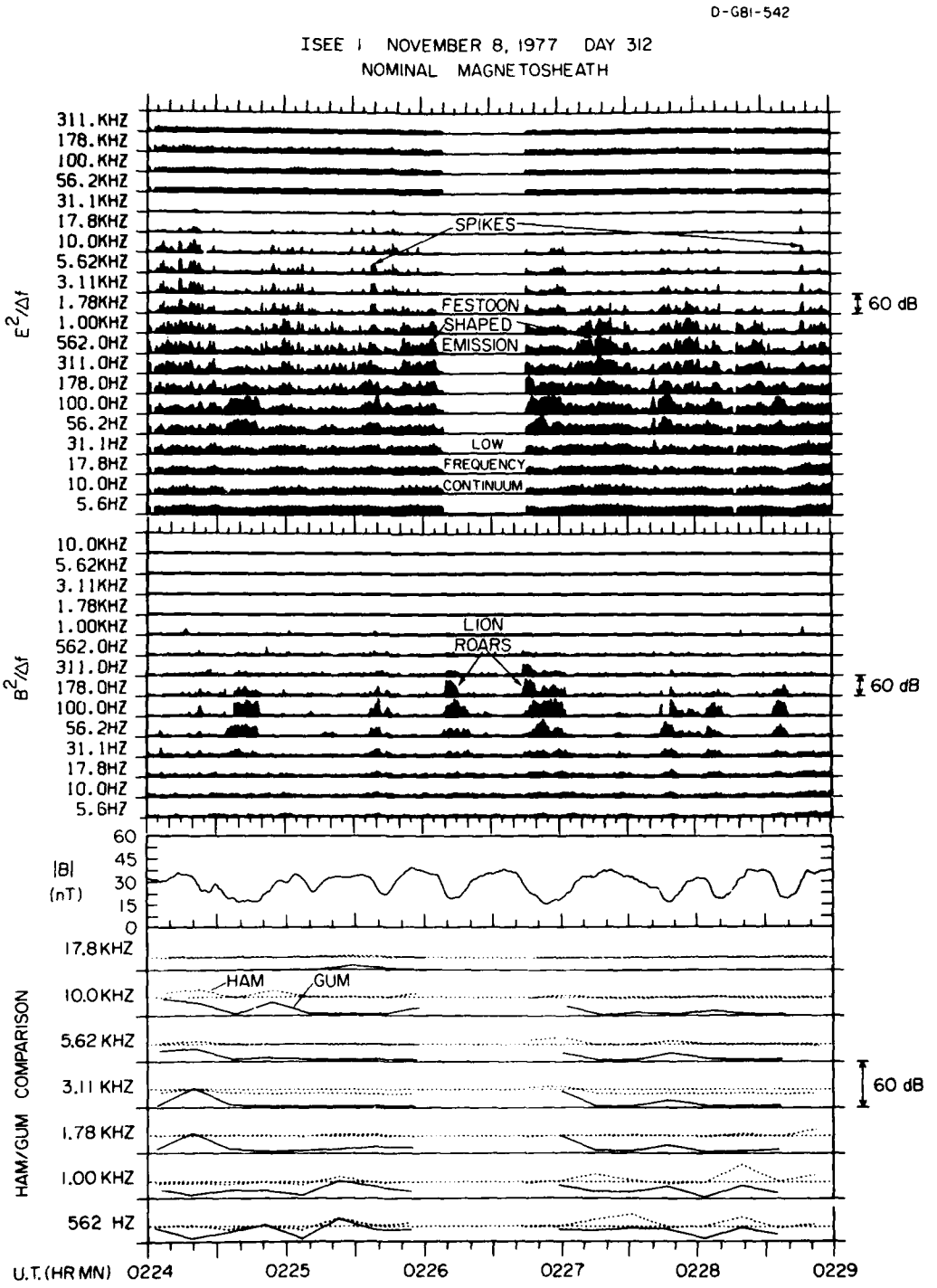
D-GBI-542
ISEE 1 NOVEMBER 8, 1977 DAY 312
NOMINAL MAGNETOSHEATH
311.KHZ
178.KHZ
100.KHZ
56.2KHZ
31.1KHZ
17.8KHZ
10.0KHZ
5.62KHZ
3.11KHZ
1.78KHZ
1.00KHZ
562.0HZ
311.0HZ
178.0HZ
100.0HZ
56.2HZ
31.1HZ
17.8HZ
10.0HZ
5.6HZ
E²/Δf
SPIKES
FESTOON
SHAPED
EMISSION
LOW
FREQUENCY
CONTINUUM
60 dB
10.0KHZ
5.62KHZ
3.11KHZ
1.78KHZ
1.00KHZ
562.0HZ
311.0HZ
178.0HZ
100.0HZ
56.2HZ
31.1HZ
17.8HZ
10.0HZ
5.6HZ
B²/Δf
LION
ROARS
60 dB
60
45
30
15
0
|B|
(nT)
17.8KHZ
10.0KHZ
5.62 KHZ
3.11 KHZ
1.78 KHZ
1.00 KHZ
562 HZ
HAM
GUM
HAM/GUM COMPARISON
60 dB
U.T.(HR MN) 0224
0225
0226
0227
0228
0229

Figure 2

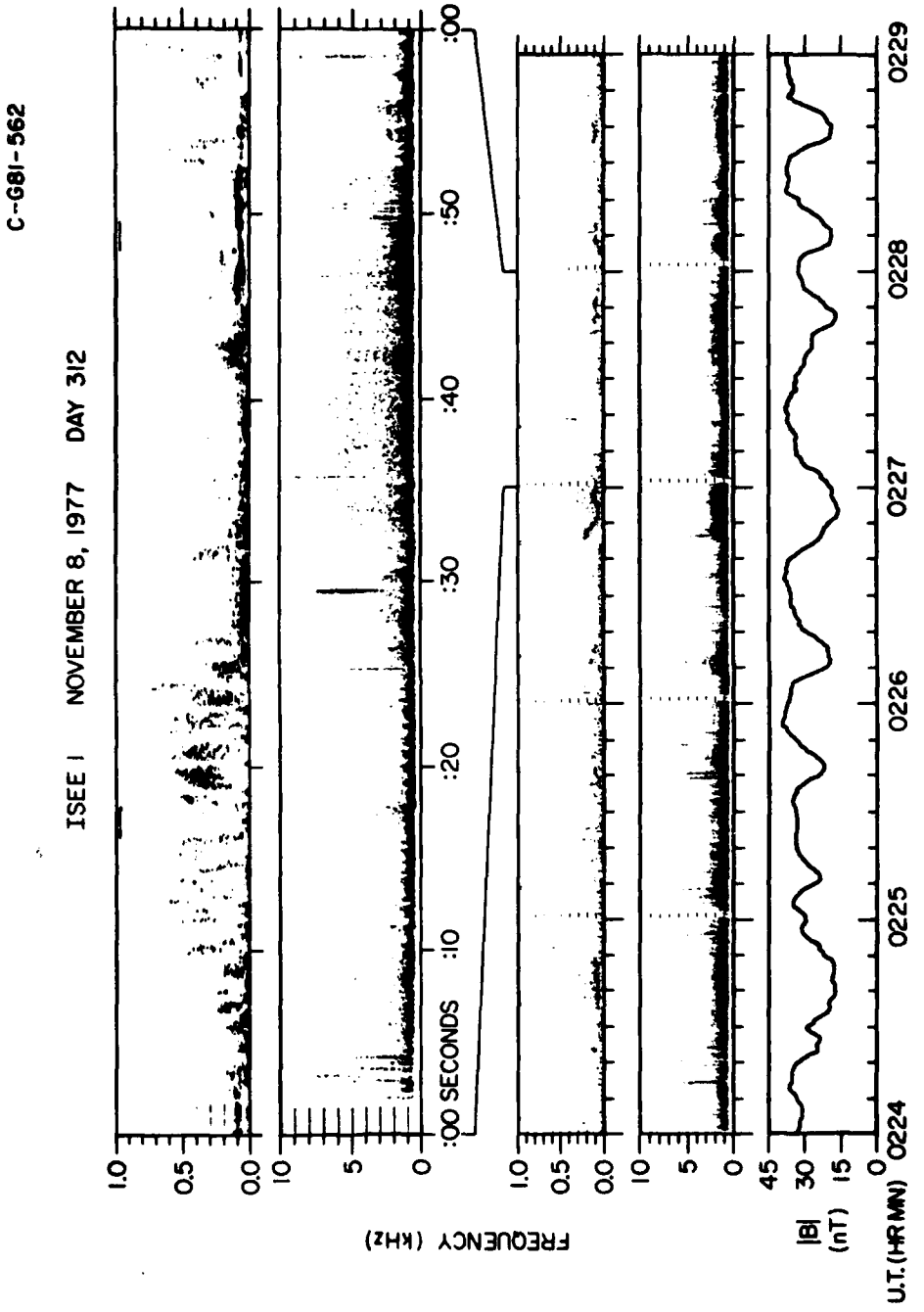
C-681-562
ISEE 1 NOVEMBER 8, 1977 DAY 312
:00 SECONDS :10 :20 :30 :40 :50 :00
FREQUENCY (kHz)
1.0
0.5
0.0
10
5
0
|B| (nT)
45
30
15
0
U.T.(HR MN) 0224 0225 0226 0227 0228 0229

Figure 3

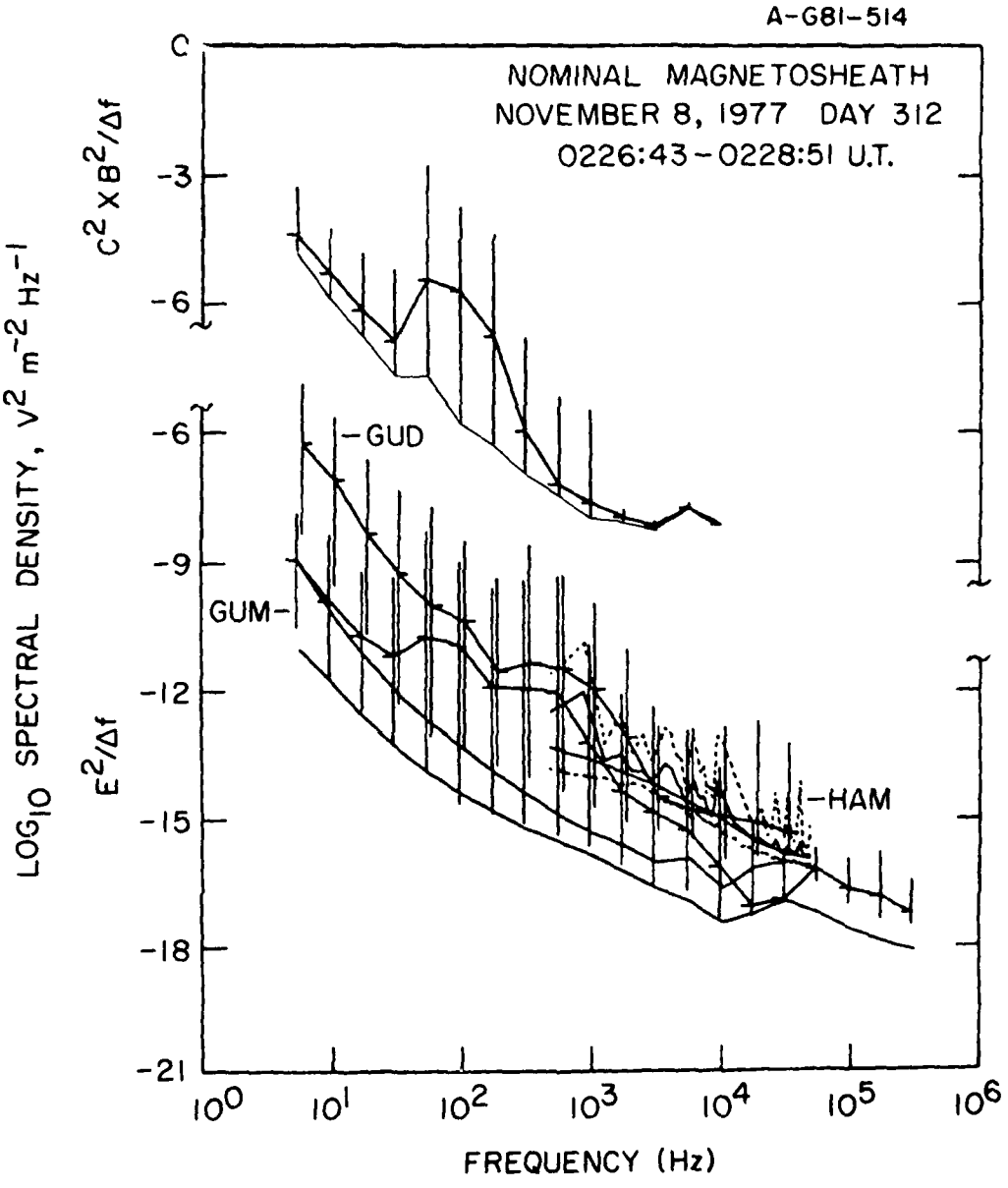
A-G81-514
NOMINAL MAGNETOSHEATH
NOVEMBER 8, 1977 DAY 312
0226:43-0228:51 U.T.
$C^2 \times B^2/\Delta f$
$E^2/\Delta f$
GUD
GUM
HAM
LOG_{10} SPECTRAL DENSITY, $V^2\ m^{-2}\ Hz^{-1}$
FREQUENCY (Hz)
0
-3
-6
-6
-9
-12
-15
-18
-21
10^0
10^1
10^2
10^3
10^4
10^5
10^6

Figure 4

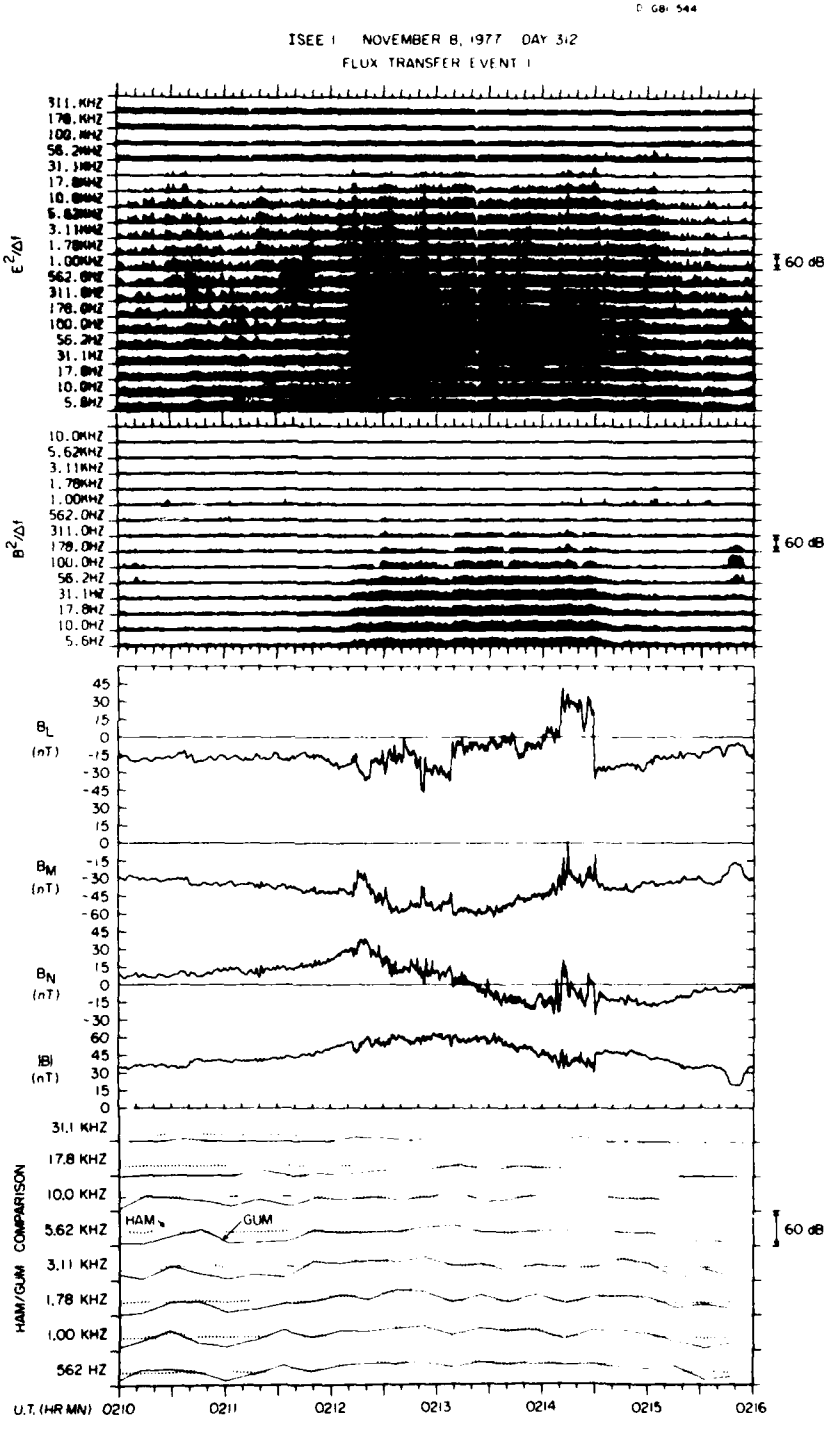
ISEE 1 NOVEMBER 8, 1977 DAY 312
FLUX TRANSFER EVENT 1
$E^2/\Delta f$
60 dB
$B^2/\Delta f$
60 dB
B_L (nT)
B_M (nT)
B_N (nT)
|B| (nT)
HAM/GUM COMPARISON
HAM
GUM
60 dB
U.T. (HR MN) 0210 0211 0212 0213 0214 0215 0216

Figure 5

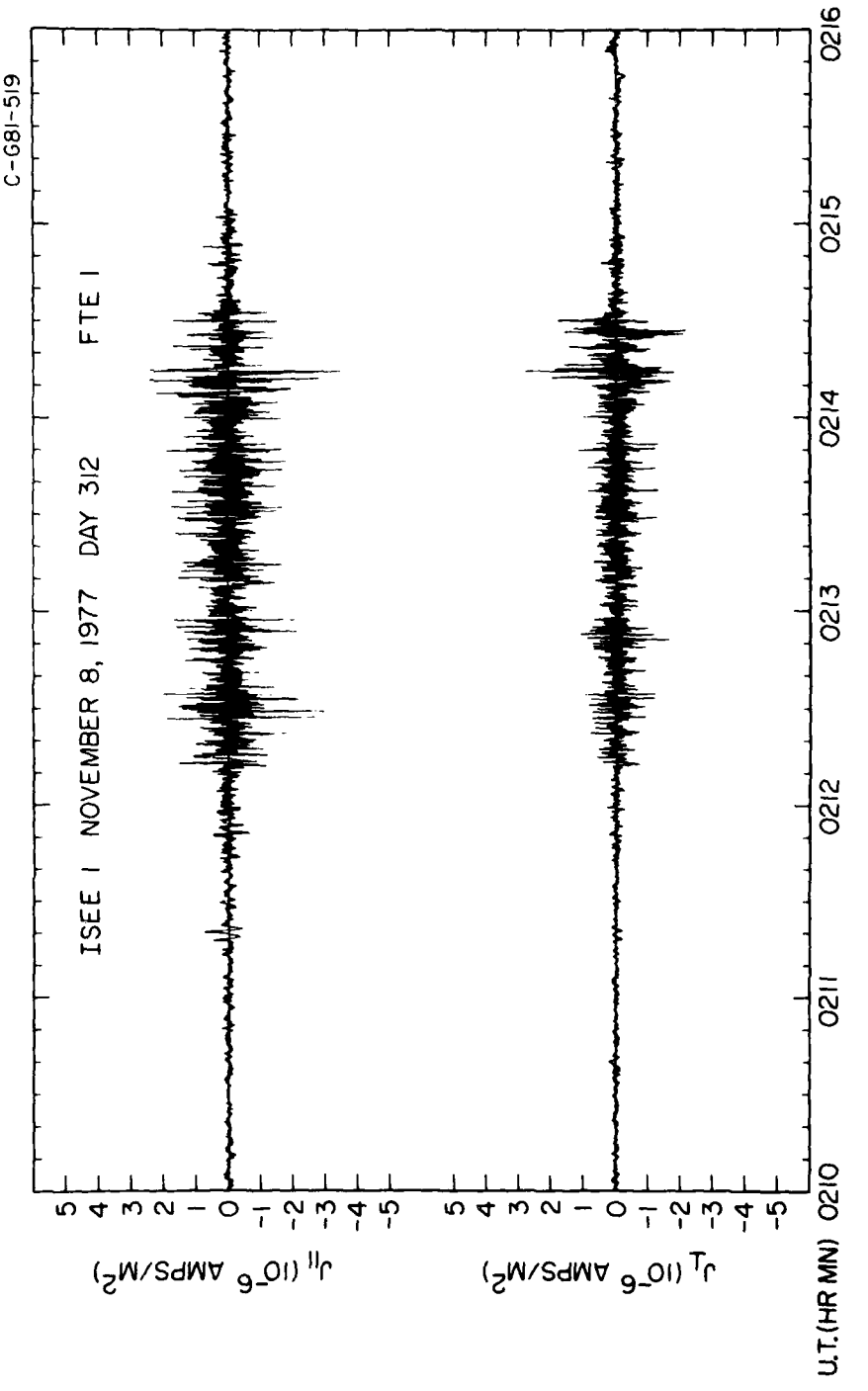
C-681-519
ISEE 1 NOVEMBER 8, 1977 DAY 312 FTE 1
$J_{\parallel}$ (10^{-6} AMPS/M^2)
$J_{\perp}$ (10^{-6} AMPS/M^2)
5 4 3 2 1 0 -1 -2 -3 -4 -5
U.T.(HR MN) 0210 0211 0212 0213 0214 0215 0216

Figure 6

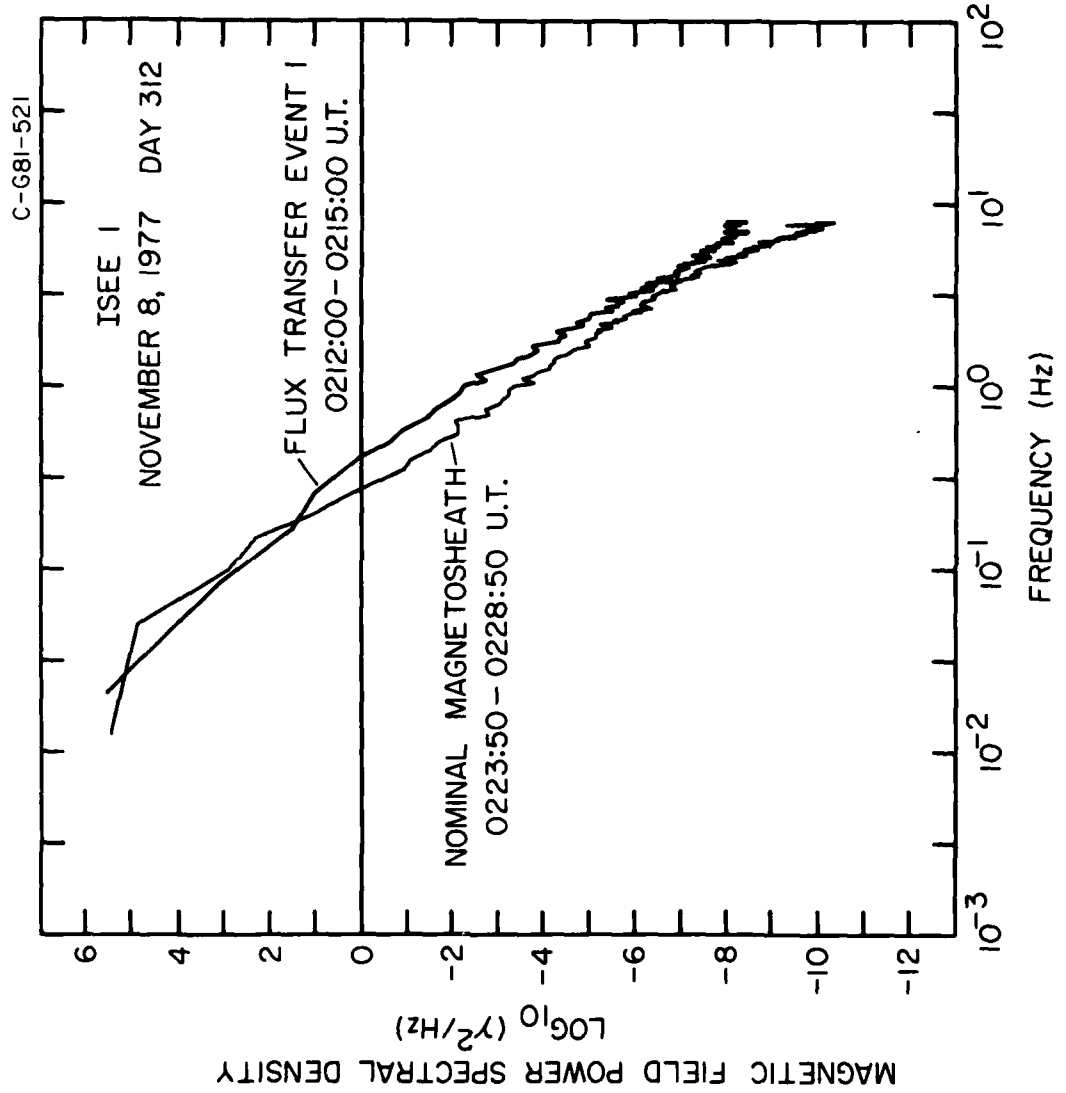
C-G81-521
ISEE 1
NOVEMBER 8, 1977 DAY 312
FLUX TRANSFER EVENT 1
0212:00-0215:00 U.T.
NOMINAL MAGNETOSHEATH
0223:50-0228:50 U.T.
MAGNETIC FIELD POWER SPECTRAL DENSITY
LOG10 (γ2/Hz)
FREQUENCY (Hz)
6
4
2
0
-2
-4
-6
-8
-10
-12
10-3
10-2
10-1
100
101
102

Figure 7

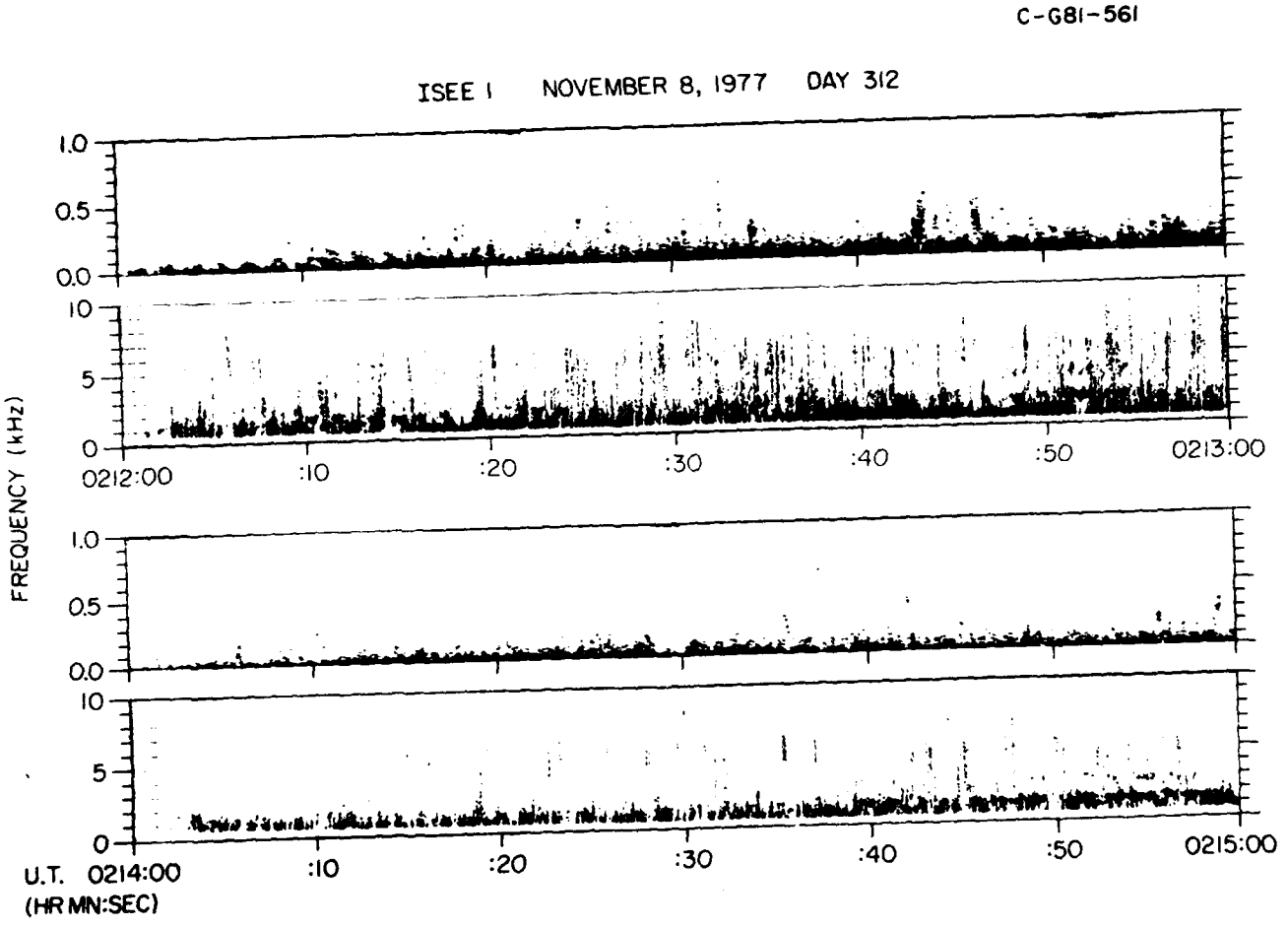
C-G81-561
ISEE 1 NOVEMBER 8, 1977 DAY 312
FREQUENCY (kHz)
1.0
0.5
0.0
10
5
0
0212:00
:10
:20
:30
:40
:50
0213:00
1.0
0.5
0.0
10
5
0
U.T. 0214:00
(HR MN:SEC)
:10
:20
:30
:40
:50
0215:00

Figure 8

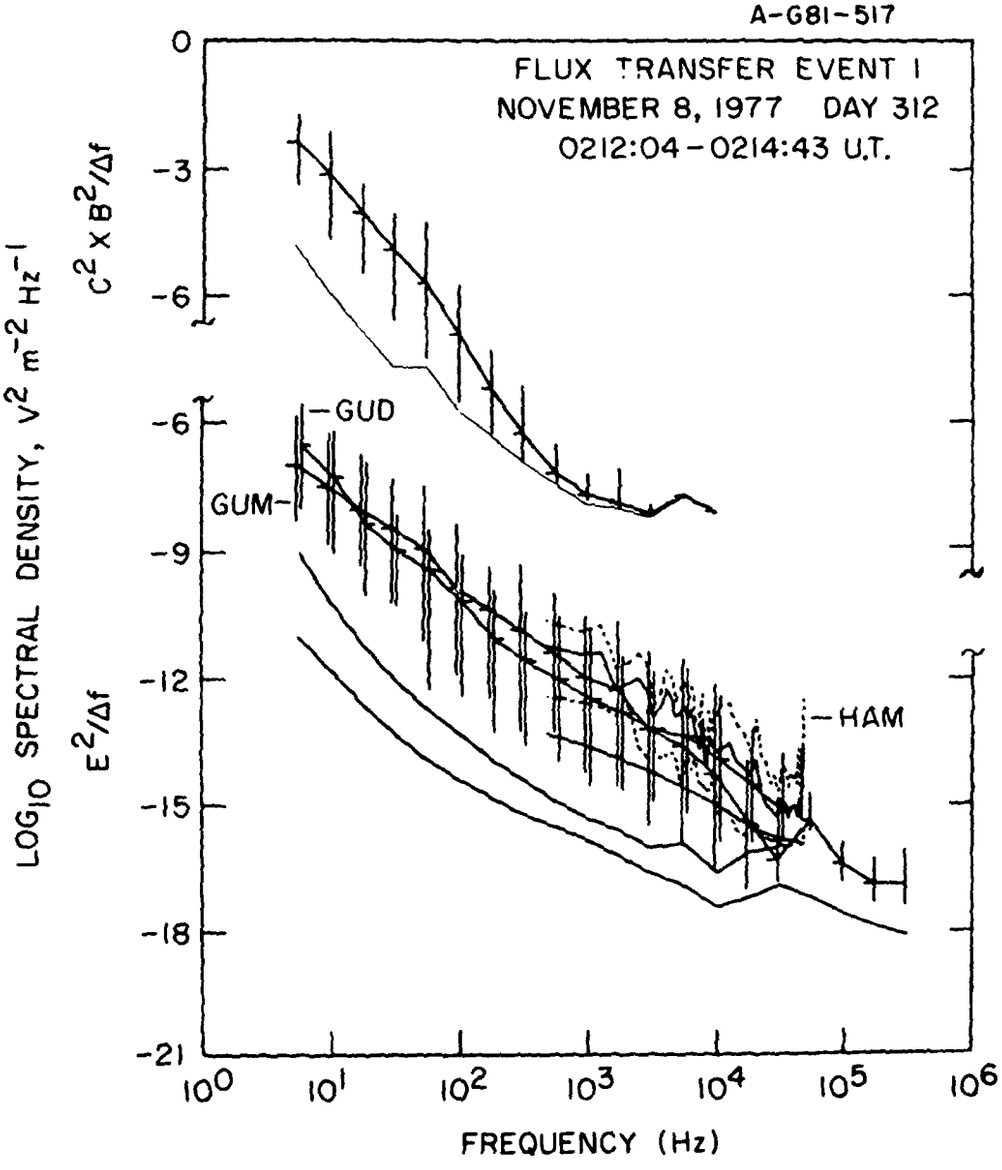
A-G81-517
FLUX TRANSFER EVENT I
NOVEMBER 8, 1977 DAY 312
0212:04-0214:43 U.T.
GUD
GUM
HAM
LOG10 SPECTRAL DENSITY, V2 m-2 Hz-1
C2 x B2/Δf
E2/Δf
0
-3
-6
-6
-9
-12
-15
-18
-21
10^0
10^1
10^2
10^3
10^4
10^5
10^6
FREQUENCY (Hz)

Figure 9

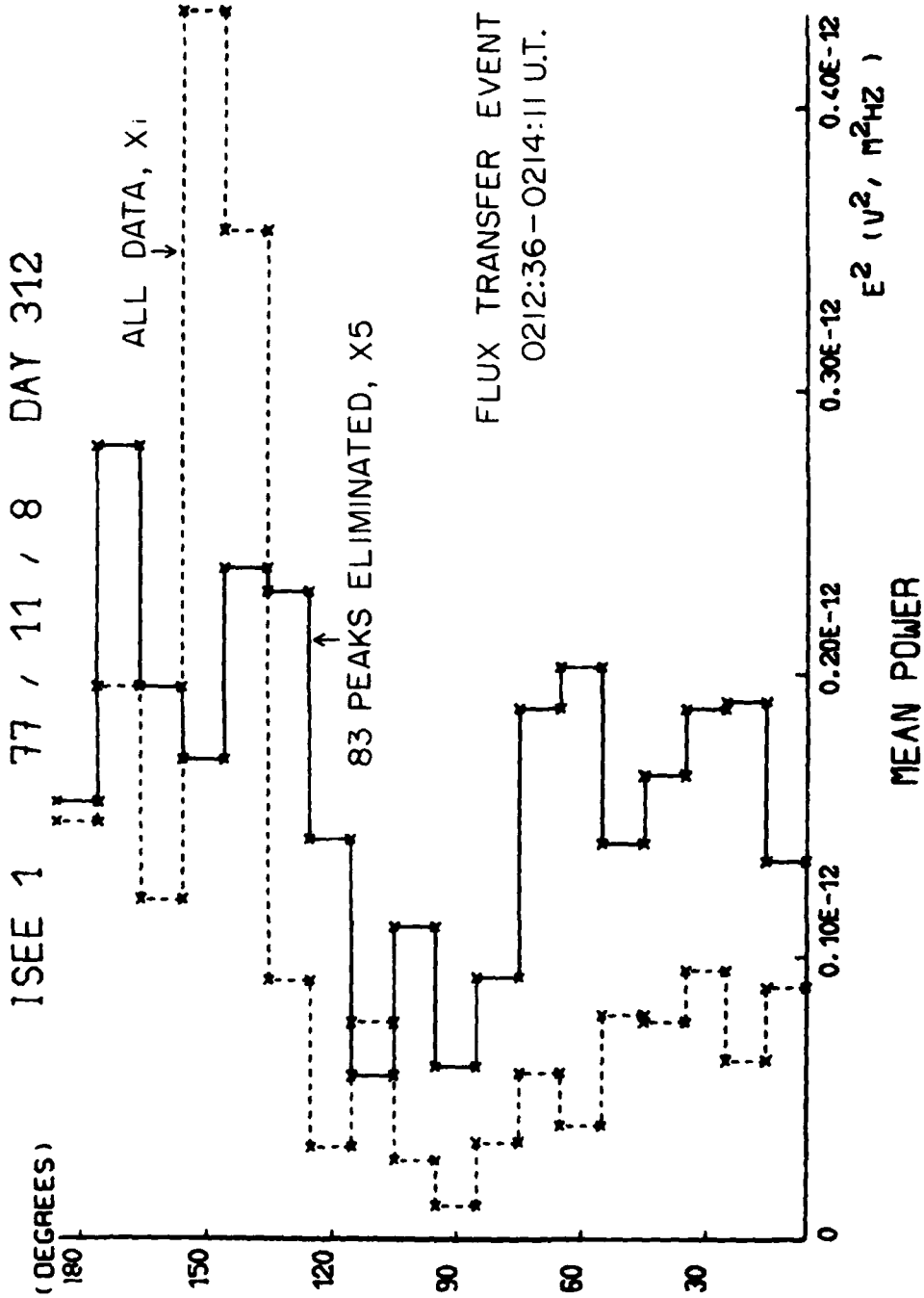
A-G81-518
ISEE 1 77 / 11 / 8 DAY 312
ALL DATA, Xi
83 PEAKS ELIMINATED, X5
FLUX TRANSFER EVENT I
0212:36-0214:11 U.T.
θ (DEGREES)
180
150
120
90
60
30
0
0.10E-12
0.20E-12
0.30E-12
0.40E-12
E² (V², M²HZ)
MEAN POWER

Figure 10

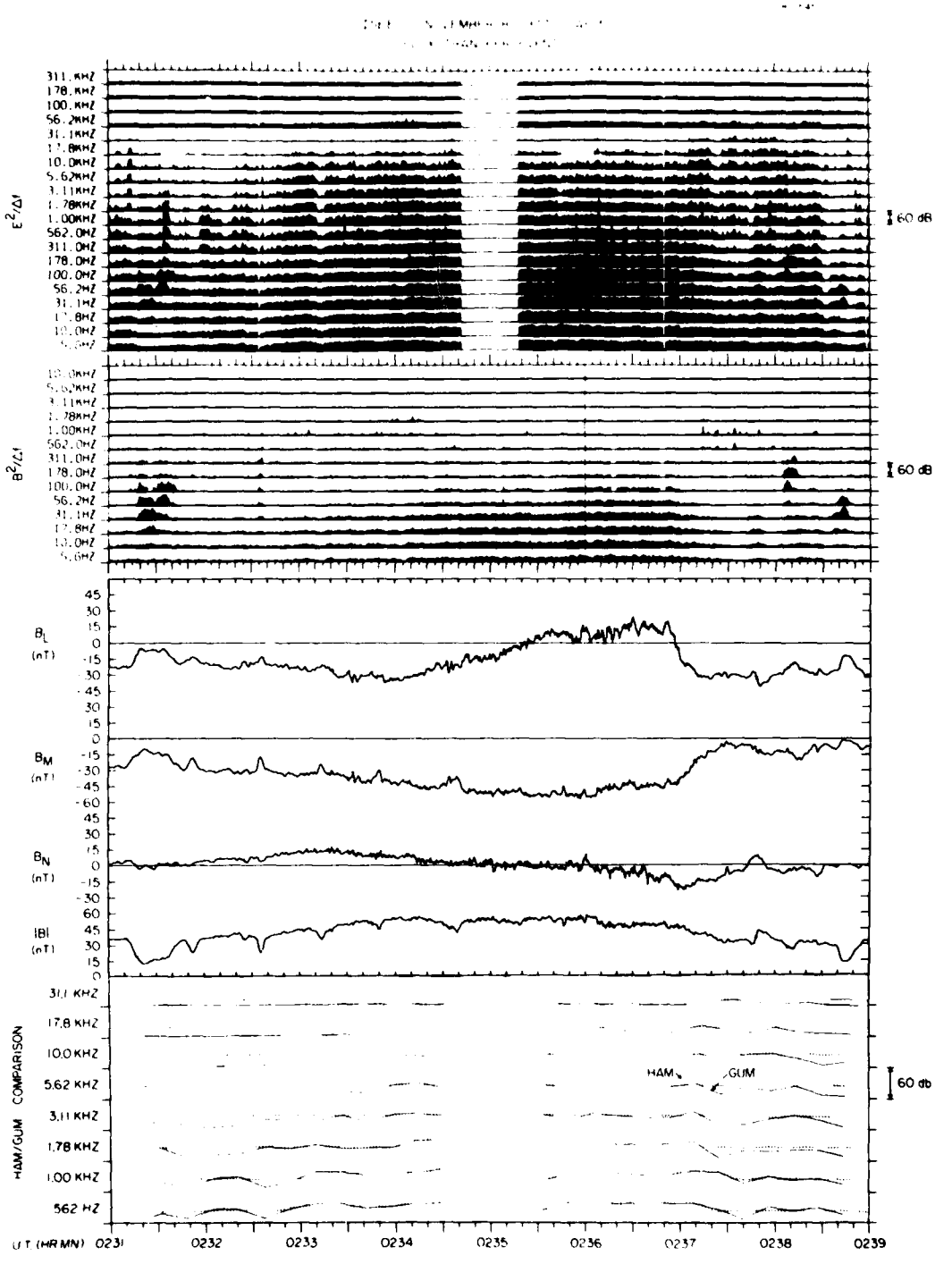
$E^2/\Delta f$
311.0HZ
178.0HZ
100.0HZ
56.2HZ
31.1HZ
17.8HZ
10.0HZ
5.62KHZ
3.11KHZ
1.78KHZ
1.00KHZ
562.0HZ
311.0HZ
178.0HZ
100.0HZ
56.2HZ
31.1HZ
17.8HZ
10.0HZ
60 dB
$B^2/\Delta f$
60 dB
B_L (nT)
B_M (nT)
B_N (nT)
|B| (nT)
HAM/GUM COMPARISON
31.1 KHZ
17.8 KHZ
10.0 KHZ
5.62 KHZ
3.11 KHZ
1.78 KHZ
1.00 KHZ
562 HZ
HAM
GUM
60 db
U.T. (HR MN) 0231
0232
0233
0234
0235
0236
0237
0238
0239

Figure 11

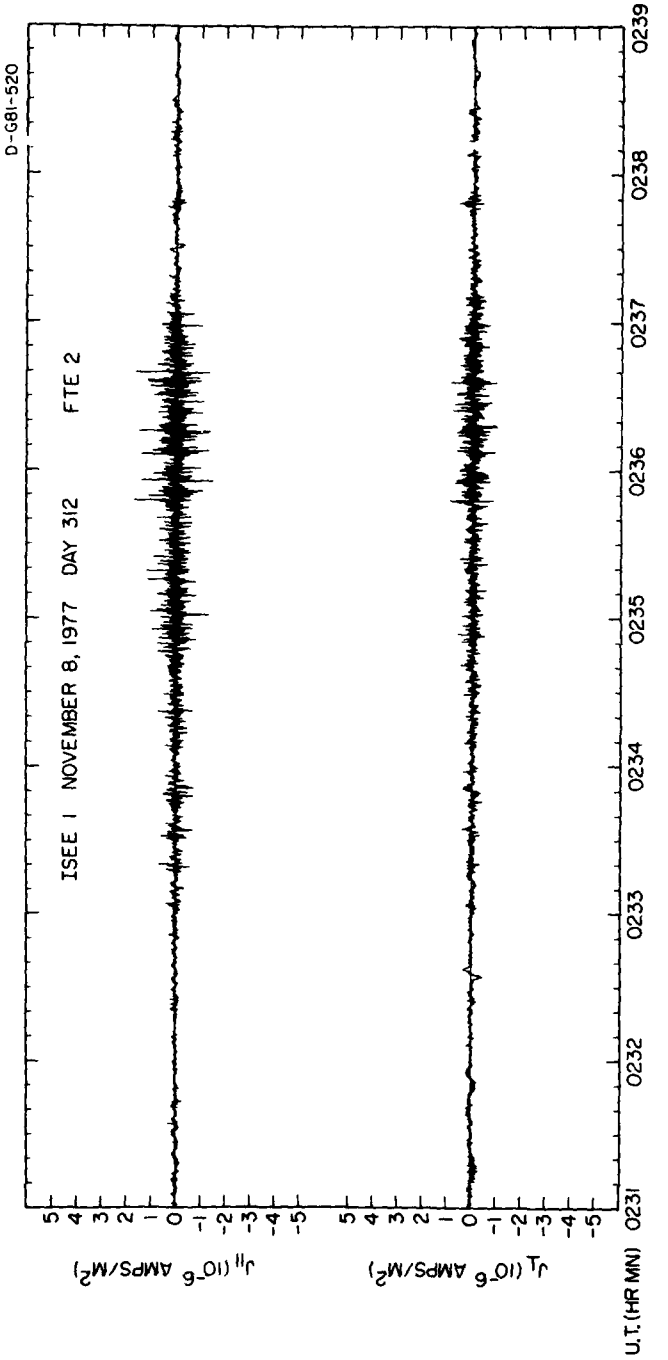
D-G81-520
ISEE 1 NOVEMBER 8, 1977 DAY 312 FTE 2
$J_{\parallel}$ (10^{-6} AMPS/M^2)
$J_{\perp}$ (10^{-6} AMPS/M^2)
U.T.(HR MN)
0231
0232
0233
0234
0235
0236
0237
0238
0239

Figure 12

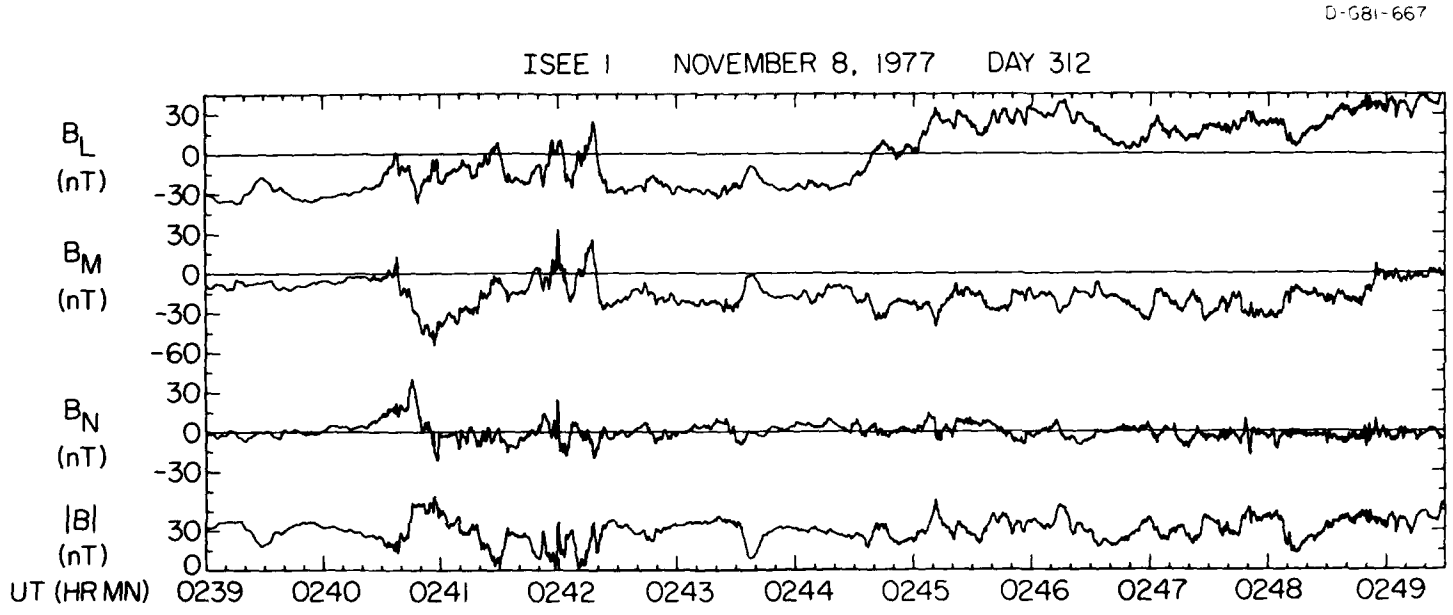
D-G81-667
ISEE 1 NOVEMBER 8, 1977 DAY 312
B_L (nT)
B_M (nT)
B_N (nT)
|B| (nT)
30
0
-30
-60
UT (HR MN)
0239
0240
0241
0242
0243
0244
0245
0246
0247
0248
0249

Figure 13

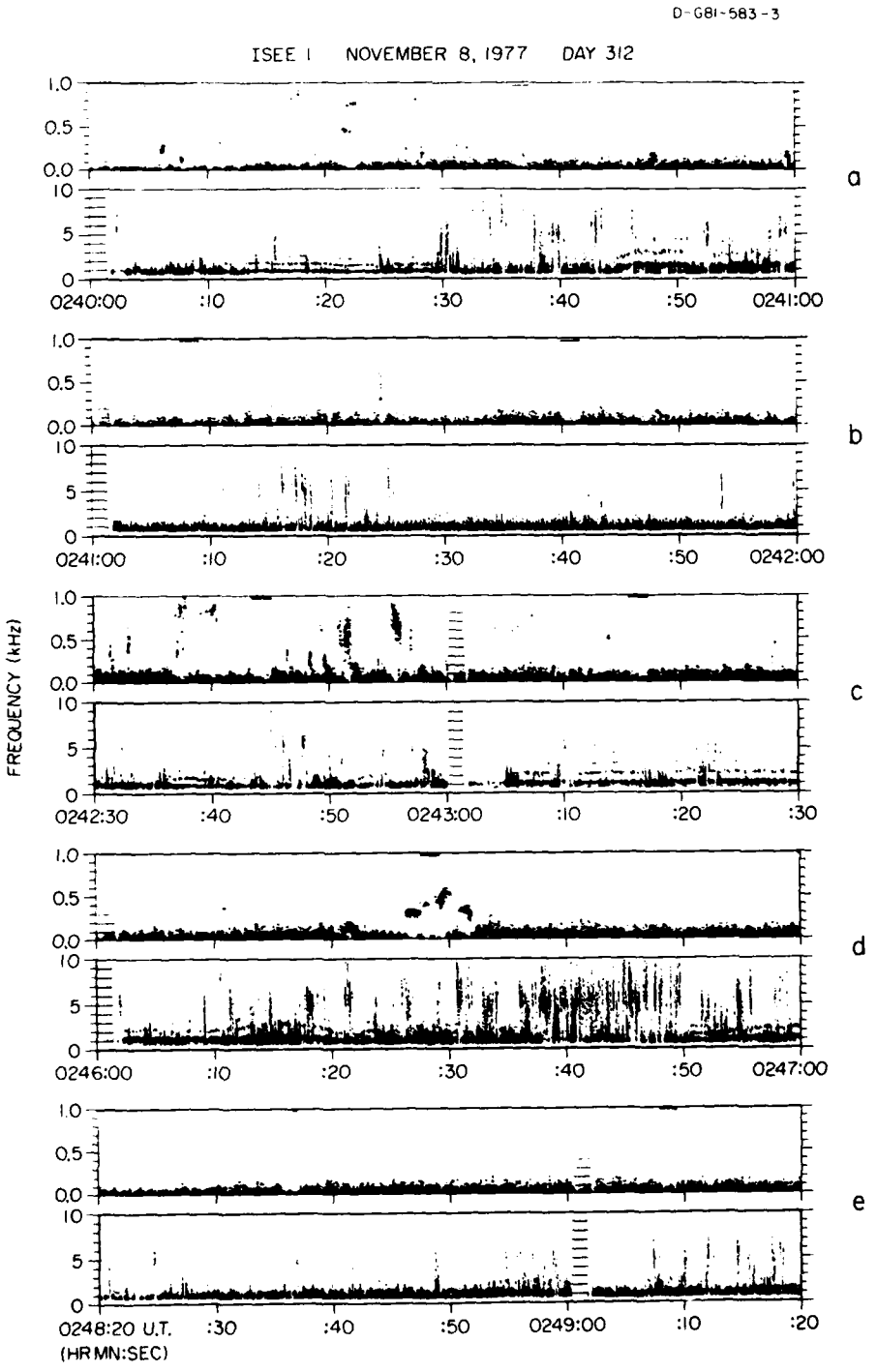
D-G81-583-3
ISEE 1 NOVEMBER 8, 1977 DAY 312
FREQUENCY (kHz)
1.0
0.5
0.0
10
5
0
a
0240:00
:10
:20
:30
:40
:50
0241:00
b
0242:00
c
0242:30
:40
:50
0243:00
:10
:20
:30
d
0246:00
0247:00
e
0248:20 U.T.
(HRMN:SEC)
0249:00

Figure 14

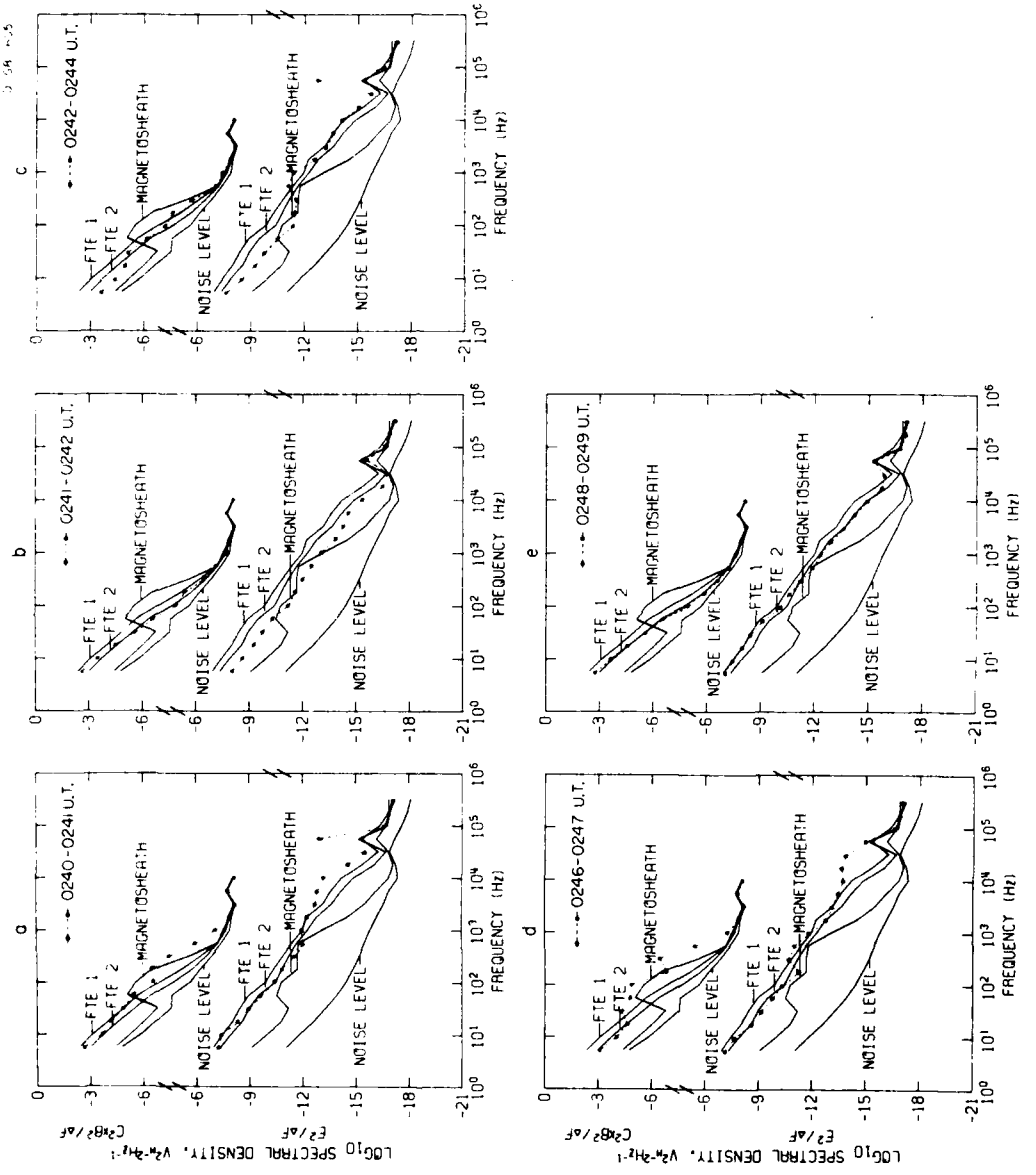
a
0240-0241 U.T.
b
0241-0242 U.T.
c
0242-0244 U.T.
d
0246-0247 U.T.
e
0248-0249 U.T.
FTE 1
FTE 2
MAGNETOSHEATH
NOISE LEVEL
FREQUENCY (Hz)
LOG10 SPECTRAL DENSITY, V2m-2Hz-1
E2/aF
C2B2/aF

Figure 15

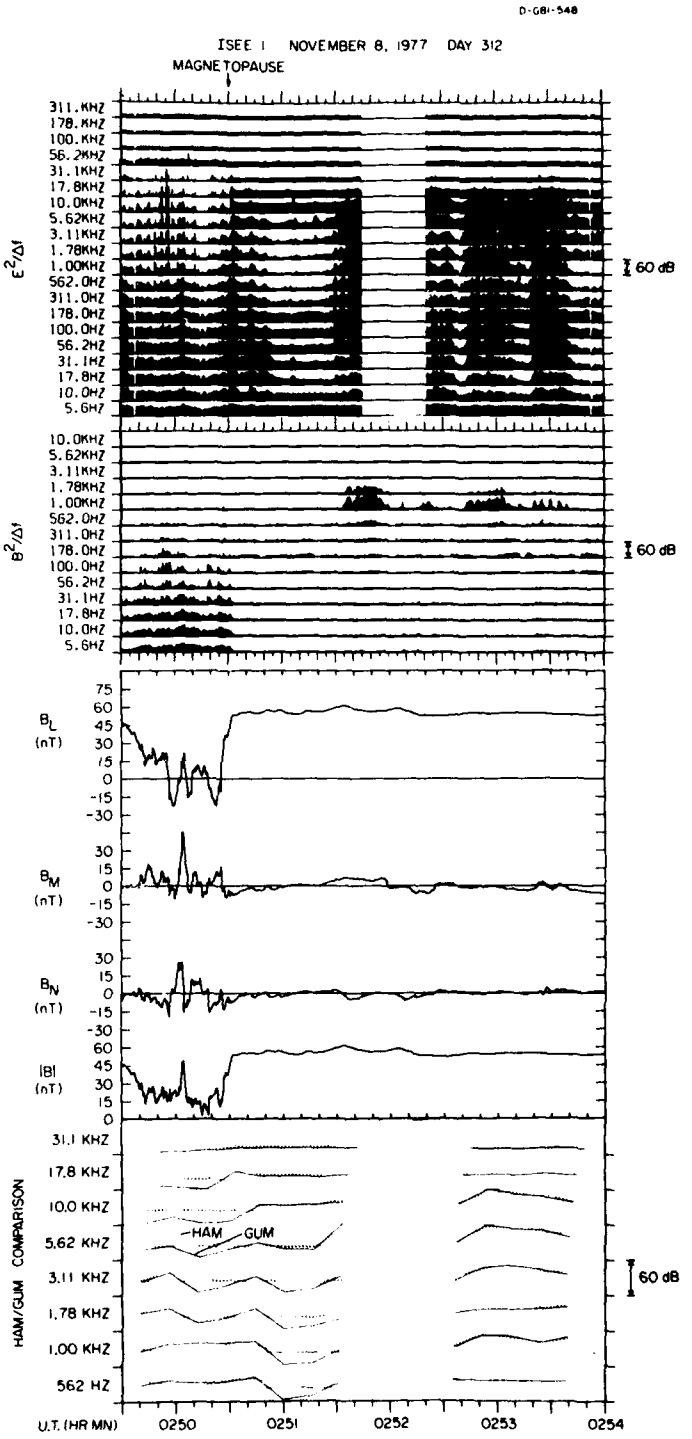
D-GBI-548
ISEE 1 NOVEMBER 8, 1977 DAY 312
MAGNETOPAUSE
311.KHZ
178.KHZ
100.KHZ
56.2KHZ
31.1KHZ
17.8KHZ
10.0KHZ
5.62KHZ
3.11KHZ
1.78KHZ
1.00KHZ
562.0HZ
311.0HZ
178.0HZ
100.0HZ
56.2HZ
31.1HZ
17.8HZ
10.0HZ
5.6HZ
E²/Δf
60 dB
10.0KHZ
5.62KHZ
3.11KHZ
1.78KHZ
1.00KHZ
562.0HZ
311.0HZ
178.0HZ
100.0HZ
56.2HZ
31.1HZ
17.8HZ
10.0HZ
5.6HZ
B²/Δf
60 dB
B_L (nT)
B_M (nT)
B_N (nT)
|B| (nT)
31.1 KHZ
17.8 KHZ
10.0 KHZ
5.62 KHZ
3.11 KHZ
1.78 KHZ
1.00 KHZ
562 HZ
HAM/GUM COMPARISON
HAM
GUM
60 dB
U.T. (HR MN)
0250
0251
0252
0253
0254

Figure 16

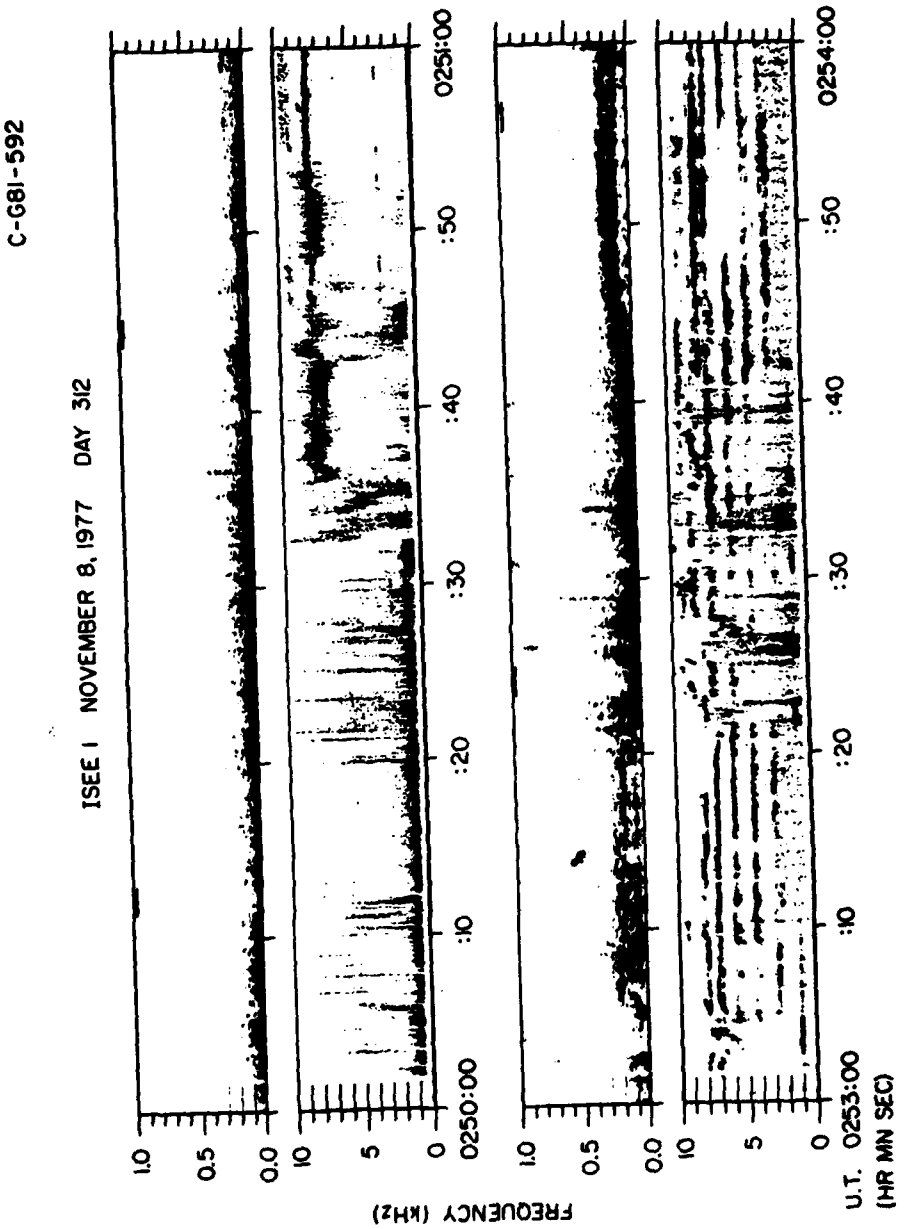
C-G81-592
ISEE I NOVEMBER 8, 1977 DAY 312
FREQUENCY (kHz)
1.0
0.5
0.0
10
5
0
0250:00
:10
:20
:30
:40
:50
0251:00
U.T. 0253:00
(HR MN SEC)
0254:00

Figure 17

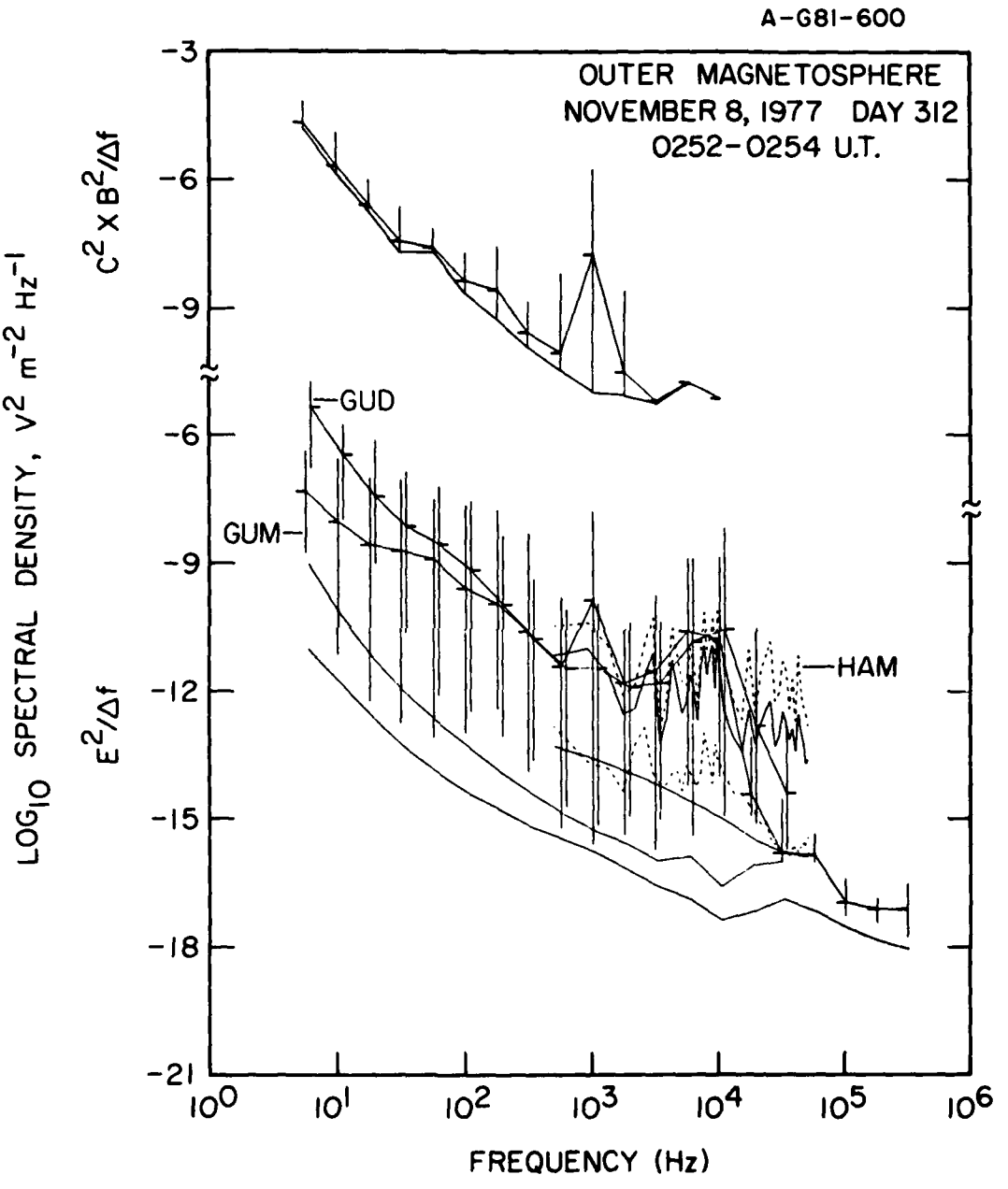
A-G81-600
OUTER MAGNETOSPHERE
NOVEMBER 8, 1977 DAY 312
0252-0254 U.T.
GUD
GUM
HAM
LOG10 SPECTRAL DENSITY, V2 m-2 Hz-1
C2 X B2/Δf
E2/Δf
-3
-6
-9
-6
-9
-12
-15
-18
-21
10^0
10^1
10^2
10^3
10^4
10^5
10^6
FREQUENCY (Hz)

Figure 18

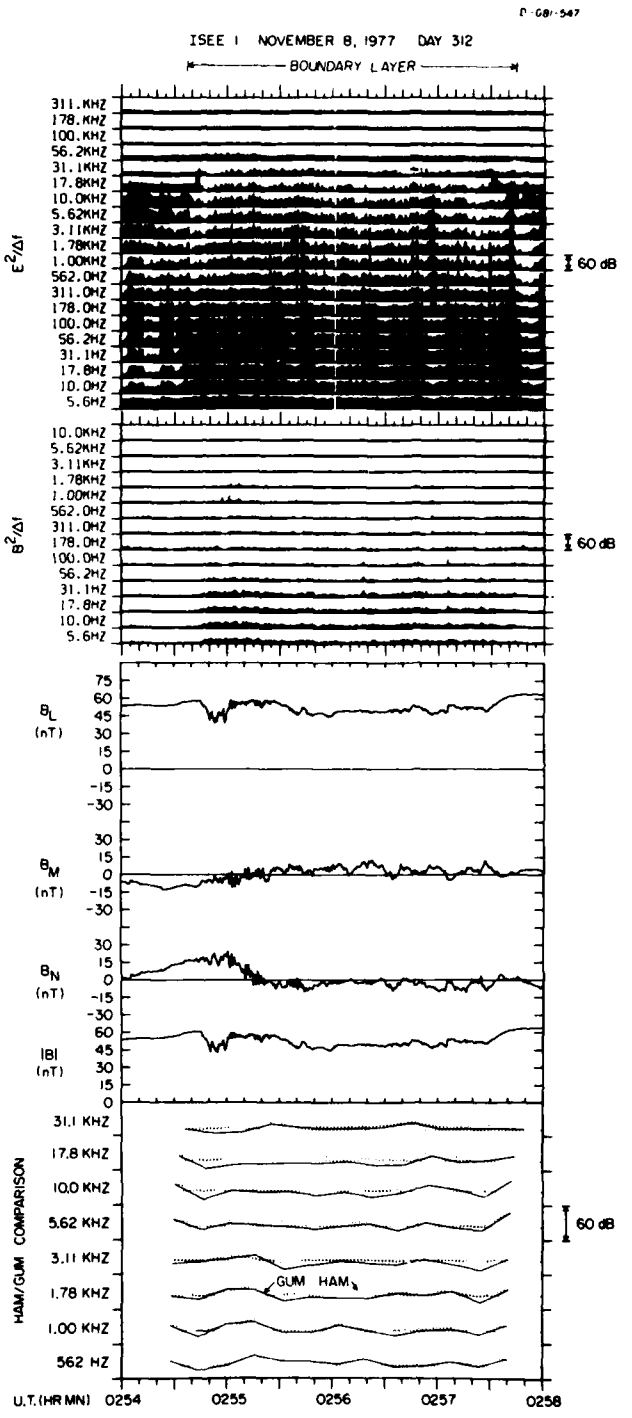
ISEE 1 NOVEMBER 8, 1977 DAY 312
BOUNDARY LAYER
311.KHZ
178.KHZ
100.KHZ
56.2KHZ
31.1KHZ
17.8KHZ
10.0KHZ
5.62KHZ
3.11KHZ
1.78KHZ
1.00KHZ
562.0HZ
311.0HZ
178.0HZ
100.0HZ
56.2HZ
31.1HZ
17.8HZ
10.0HZ
5.6HZ
E²/Δf
60 dB
10.0KHZ
5.62KHZ
3.11KHZ
1.78KHZ
1.00KHZ
562.0HZ
311.0HZ
178.0HZ
100.0HZ
56.2HZ
31.1HZ
17.8HZ
10.0HZ
5.6HZ
B²/Δf
60 dB
B_L (nT)
B_M (nT)
B_N (nT)
|B| (nT)
31.1 KHZ
17.8 KHZ
10.0 KHZ
5.62 KHZ
3.11 KHZ
1.78 KHZ
1.00 KHZ
562 HZ
HAM/GUM COMPARISON
GUM
HAM
60 dB
U.T.(HR MN) 0254 0255 0256 0257 0258

Figure 19

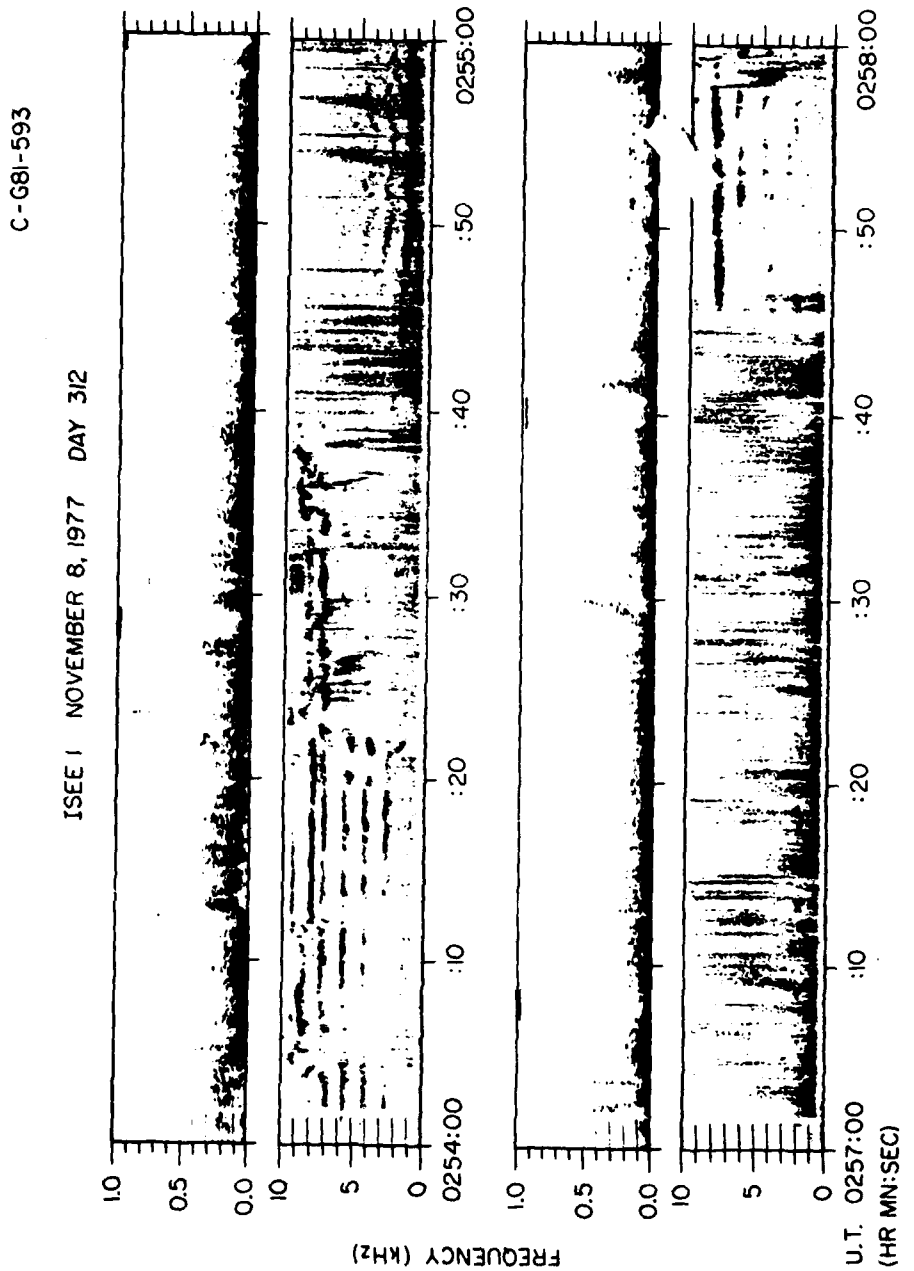
C-G81-593
ISEE 1 NOVEMBER 8, 1977 DAY 312
1.0
0.5
0.0
10
5
0
0254:00
:10
:20
:30
:40
:50
0255:00
FREQUENCY (kHz)
U.T. 0257:00
(HR MN:SEC)
0258:00

Figure 20

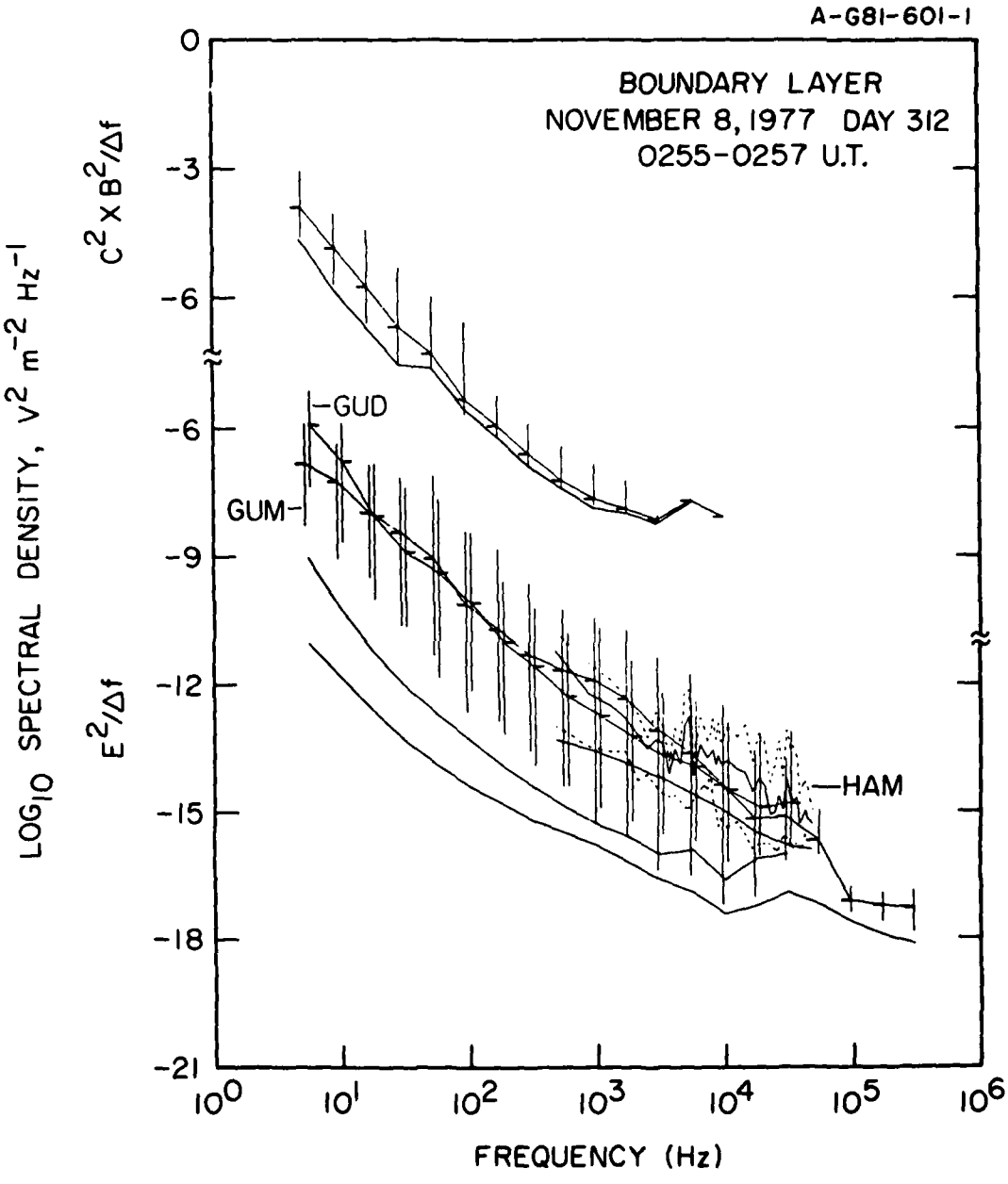
A-G81-601-1
BOUNDARY LAYER
NOVEMBER 8, 1977 DAY 312
0255-0257 U.T.
LOG10 SPECTRAL DENSITY, V2 m-2 Hz-1
C2 X B2/Δf
E2/Δf
GUD
GUM
HAM
0
-3
-6
-6
-9
-12
-15
-18
-21
10^0
10^1
10^2
10^3
10^4
10^5
10^6
FREQUENCY (Hz)

Figure 21